INTEGRATED APPROACHES TO OPTIMAL MULTI-PERIOD DESALINATION SYNTHESIS INVOLVING WATER-ENERGY NEXUS

A Dissertation

by

HASSAN MOHAMMED O. BAAQEEL

Submitted to the Office of Graduate and Professional Studies of
Texas A&M University
in partial fulfillment of the requirements for the degree of

DOCTOR OF PHILOSOPHY

Chair of Committee,	Mahmoud El-Halwagi
Committee Members,	M. Sam Mannan
	Sergiy Butenko
	Hisham Nasr-El-Din
Head of Department,	M. Nazmul Karim

August 2018

Major Subject: Chemical Engineering

ABSTRACT

This work develops novel tools for the multi-period and multiscale synthesis of water desalination systems for systematically optimizing the benefits of the integration of emerging desalination technologies and the water-energy nexus. The research develops the optimization frameworks for the following problems: (1) optimization of multi-effect distillation (MED) design via MD brine treatment and process heat integration, (2) synthesis of desalination systems for multi-period capacity planning, and (3) synthesis and scheduling of solar-assisted membrane distillation (MD) for domestic water desalination. To solve the three problems, the water-energy nexus must be addressed in the planning, design, and operation of the water desalination system.

In the first problem, an optimization approach to the design of MED-MD in the context of water-energy nexus with an industrial process is developed. The hybrid MED-MD desalination system is thermally integrated with industrial facility while any additional required thermal energy is supplied from external sources. The optimization framework targets optimizing the operating and design variables of the MED and MD units as well as the excess heat extracted from the industrial facility.

In the second problem, an optimization approach was used to identify the optimal capacity planning of distressed water desalination systems considering the integration of emerging desalination technologies. Despite the economic challenges many emerging technologies face, some new desalination technologies such as MD demonstrate promising candidacy in the optimal expansion of desalination systems due to their modularity and other advantages. The developed framework also addresses the multiscale nature of the problem. Unit-specific decision variables

such as the top brine temperature (TBT) and MD recycle ratio are simultaneously optimized with the synthesis of the multi-period flowsheet.

In the third problem, a systematic approach for the design and scheduling of a skid-mounted solar-assisted membrane distillation system is developed. The problem targets domestic water demand in remote areas that are not supported by fresh water infrastructure. The proposed system consists of both thermal and photovoltaic (PV) solar systems to provide the energy required for desalination and system's equipment. Storage tanks are used to collect thermal energy and to supply the feed to the MD system while PV cells are connected to electric-energy storage batteries to drive the pumping. Conventional fossil fuel is used to supplement the solar thermal energy as needed. The aim of the optimization framework is to determine the number and size of the storage tanks, the operating variables, the collection and dispatch times, the extent of solar and fossil-energy uses, and the operating schedule for the integrated system.

The merits of the developed frameworks are illustrated in three distinct case studies with clear focus on MD as an example of emerging technologies integrated with conventional technologies. In all the three case studies, MD desalination as a standalone solution was suboptimal when compared to conventional desalination technologies. However, with the introduction of water-energy nexus with adjacent processing facilities and solar thermal heating, interesting results evolved with MD as a constituent of the global optimum. In addition, emerging technologies have shown economic merits when utilized at the end of the planning horizon in expanding systems, due to its modularity.

DEDICATION

This dissertation is dedicated to my parents, Mohammed and Fatimah, who instilled in me the love of knowledge and that learning lasts from cradle to grave. To my wife, this would have never been possible without your help. This achievement goes to you, so allow me to call you Dr. Sarah. Lastly, a special dedication to my lovely kids: Mohammed, Albaraa, and Danah. Without you, this journey would have been shorter but less enjoyable.

ACKNOWLEDGEMENTS

My deep gratitude goes, first, to my professor, Dr. Mahmoud El-Halwagi, for his continuous support and help in this work. His guidance and insights have been instrumental to this accomplishment. I feel privileged to have him as an advisor in my PhD, with his invaluable expertise and knowledge. My work with Dr. El-Halwagi has also left a dent on me on a personal level. His insights on leadership, teamwork, values, and scientific progress have found a flourishing ground in me. For all of that, my wholehearted thanks go to him.

My sincere appreciation, also, goes to my committee members who have spared the time and effort to critique my work, provide constructive feedback, and share their expertise. They are Dr. M. Sam Mannan, Dr. Sergiy Butenko, and Dr. Hisham Nasr-El-Din.

Special acknowledgement and thanks is due to collaborating scholars in this work from other research institutions, namely King Abdullah University of Science and Technology (KAUST) and King Abdulaziz University. Their contribution has added enlightening element to my research through their experimental work in water desalination.

From my research group, I would like to thank specific researchers for their help and insightful discussions. Thank you Dr. Rajib Mukherjee, Dr. Debalina Sengupta, Dr. Nesreen El-Sayed, Mr. Kevin Topolski, and Dr. Fahad Al-Fadhli.

CONTRIBUTORS AND FUNDING SOURCES

This work was supported by a dissertation committee consisting of Professors Mahmoud El-Halwagi and M. Sam Mannan of the Department of Chemical Engineering and Professor Hisham Nasr-El-Din of the Department of Petroleum Engineering and Professor Sergiy Butenko of the Department of Industrial Engineering.

The analyses depicted in Chapters II and the experimental validation in Chapter IV were conducted in part by Dr. Faissal Abdelhady and Dr. Hisham Bamufleh from King Abdulaziz University, Jeddah, Saudi Arabia. All other work conducted for the dissertation was completed by the student independently.

There are no outside funding contributions to acknowledge related to the research and compilation of this document.

TABLE OF CONTENTS

Page

LIST OF FIGURES

Page

LIST OF TABLES

Page

CHAPTER I

INTRODUCTION

1.1 Overview

Ranked second following climate change, access to clean water is listed by the Millennium Project as one of the greatest global challenges facing humanity (Glenn, Gordon, & Florescu, 1997) . Despite the abundance of water in our planet, 96% of earth's water is saline and unfit for human consumption. Currently, over one-third of the world's population resides in a water-stress region (Elimelech & Phillip, 2011). In some accounts, the threshold for water scarcity is defined by access to a minimum of 1,700 m^3/person per year of clean water (Rijsberman, 2006). Yet, water consumption extends beyond drinking and urban uses to both agricultural and industrial uses. Only about 12% of the world-total water withdrawal is utilized by the domestic sector while the remaining goes to the agricultural and industrial sectors (Nations, 2014). With the world population expected to exceed 10 billion by 2060 (Development, 2017), a cost-effective strategies to the production and consumption of water in all sectors appear a key requisite to the sustenance of the world economic growth and human development.

One conventional solution to the water-shortage problem is water desalination. The abundant salt water (i.e. brackish, saline, and seawater) is separated from contaminants using a wide range of separation technologies. Desalination technologies are sometime classified into three primary categories: thermal, membrane, and chemical technologies. In thermal technologies such as multi-stage flashing (MSF) and multi-effect distillation (MED), water is separated from salts and contaminants through phase separation driven by thermal energy, while chemical technologies, such as electrodialysis and water softening, rely on chemical reactions to achieve the

desired separation. Membrane processes, such as reverse osmosis (RO) and nano-filtration utilize microporous membrane for the separation.

However, water desalination is inherently (1) energy demanding and (2) capital intensive. Despite the absolute low thermodynamic minimum energy required for desalination (i.e. 1.06 kWh/m^3) (Elimelech & Phillip, 2011), actual energy consumption for water desalination is much higher. The average energy consumptions for membrane-based RO desalination is about 6 kWh/m^3 while it is in the verge of 14 kWh/m^3 for most thermal processes (Subramani, Badruzzaman, Oppenheimer, & Jacangelo, 2011). Corroborating the second characteristics of desalination processes (e.g. capital intensity), capital expenditure represents 30-40% of the overall annualized cost of desalination processes (Ghaffour, Missimer, & Amy, 2013).

The above characterization of water desalination is the motivation of this research. It stipulates the two strategies for this research to achieve better efficacy of water desalination. First, the reduction of desalination system's energy cost by tapping into water-energy nexus opportunities. Second, a cost-effective strategy for water capacity planning in desalination systems for higher capital productivity. In the next section, each of the two strategies is discussed in depth.

1.1.1 Water-Energy Nexus

The term water-energy nexus is coined to describe interlinked relationship between water and energy consumption and production in systems. To illustrate this relationship, water treatment and transport account for 8% of global energy usage. On the other hand, energy systems consume about 15% of global water withdrawals (Garcia & You, 2016).

In many process design applications, water-energy nexus is an important framework to consider to appropriately account for the complexity and interconnectivity of the two systems.

Such implications would not be accounted for if the two systems were designed separately. Of more importance to this research, water-energy nexus brings about many opportunities for cost efficacy through the various methodologies of integration (i.e. mass, heat, and property integrations). The average desalination operating cost accounts for 60-70% of the total cost of water in desalination, hence, better exploitation of water-energy nexus can yield substantial reduction in the energy cost for water production while simultaneously bearing additional advantages to the energy system.

In water desalination, much research is carried on the analysis and optimization of desalination in systems involving water-energy nexus. Gabriel et al. (2014) has analyzed water-energy nexus in GTL processes comparing different syngas technologies. Gabriel, El-Halwagi, and Linke (2016) also proposed an integrated hybrid design of MD desalination with the heat and power processes of industrial systems. González-Bravo, Elsayed, Ponce-Ortega, Nápoles-Rivera, and El-Halwagi (2015) sought modeling the synthesis of MD desalination with heat exchanger network design. Al-Aboosi and El-Halwagi (2018) has developed a framework for the optimization of water and energy systems in shale-gas production while considering multiple energy sources, cogeneration process, and water desalination.

1.1.2 Cost-Effective Capacity Planning

The total capital spent on water desalination projects to cope with the world's increasing demand is estimated over 17 billion dollars in 2016 (Subramani et al., 2011). The investment in water resources is yet to increase in the future due to the population growth and retirement of existing desalination systems. With many of the desalination plants built in the 60s and 70s (i.e. the first MSF desalination was built in 1960 in Shuwaikh, Kuwait and in Guernsey, Channel

Island) (H. T. El-Dessouky & Ettouney, 2002), they are expected to retire in the near future. The long-term planning of the investment in desalination is instrumental to a cost-effective water production. Capacity planning, in the context of this research, covers the question of what desalination plants to construct, what size, when to construct, and how to design them (i.e. optimal intra-process design).

1.1.3 Emerging Water Desalination Technologies

Another perspective of desalination technologies classifies desalination technologies into conventional and emerging technologies. This prospective is deemed important in our research as it sheds light on a group of technologies, typically overlooked in process design due to their poor economics. However, these technologies, through hybridization with conventional technologies, can be very economical in the frameworks presented in this research, namely water-energy nexus and capacity planning.

1.2 Process Background

The approach developed in this research is integral in nature. It exploits the value of integrating different desalination technologies to bridge water scarcity. The following is a description of selected conventional and emerging desalination technologies. Many of these technologies are either the subject of the research problem statement or the case study. The review covers three major thermal desalination technologies. This discussion is a precursor to the discussion on hybridization/integration of desalination technologies at the end of this section.

1.2.1 Multi-Effect Distillation (MED)

The multi-effect distillation (MED) is a thermal desalination process that utilizes external source of heat to separate water from solutes in the feed water through evaporation. To improve thermal efficiency, successive evaporators are operated at a diminishing pressure, where evaporators (except the first externally-driven evaporator) utilizes the vapor stream from the preceding evaporator as a heat source. MED comes in different design configurations, the famous of which are: feed-forward MED and parallel-feed MED.

The temperature at the first evaporator is key in the performance of the unit and referred to as the top brine temperature (TBT). TBT variation results in little impact on the efficiency of the unit, but it results in a drastic reduction in the evaporator's specific heat transfer area (Andrea Cipollina, Micale, & Rizzuti, 2009). MED is generally limited in the maximum TBT temperature when compared to its competitive technology, MSF. Budhiraja and Fares (2008) stipulates MED TBT to range from 60-65C, Alasfour, Darwish, and Amer (2005) from 60-70C, and H. T. El-Dessouky and Ettouney (2002) from 60-100C. The limitation is caused by heavy precipitation of calcium sulfate and other scaling precipitants. High-temperature multi-effect distillation (HT-ME) has been reported in literature to alleviate the scaling problem by the use of special acid treatment (Al-Shammiri & Safar, 1999; Ophir & Lokiec, 2004). In addition to scaling, high TBT temperature requires a higher quality heat source, which may be more expensive depending on the energy system in the water-energy nexus.

Another key design parameter in MED is the number of evaporative effects. Higher number of effects allow for better extraction of thermal heat from the external heat source improving the thermal efficiency of the unit, although at higher capital cost. The tradeoff between higher thermal efficiency (e.g. lower operating cost) and lower capital cost signifies an optimization problem,

exploited in most MED designs. The maximum number of evaporative effects is limited by a minimum temperature difference between effects. Figure 1 is an illustration of the feed-forward MED plant.

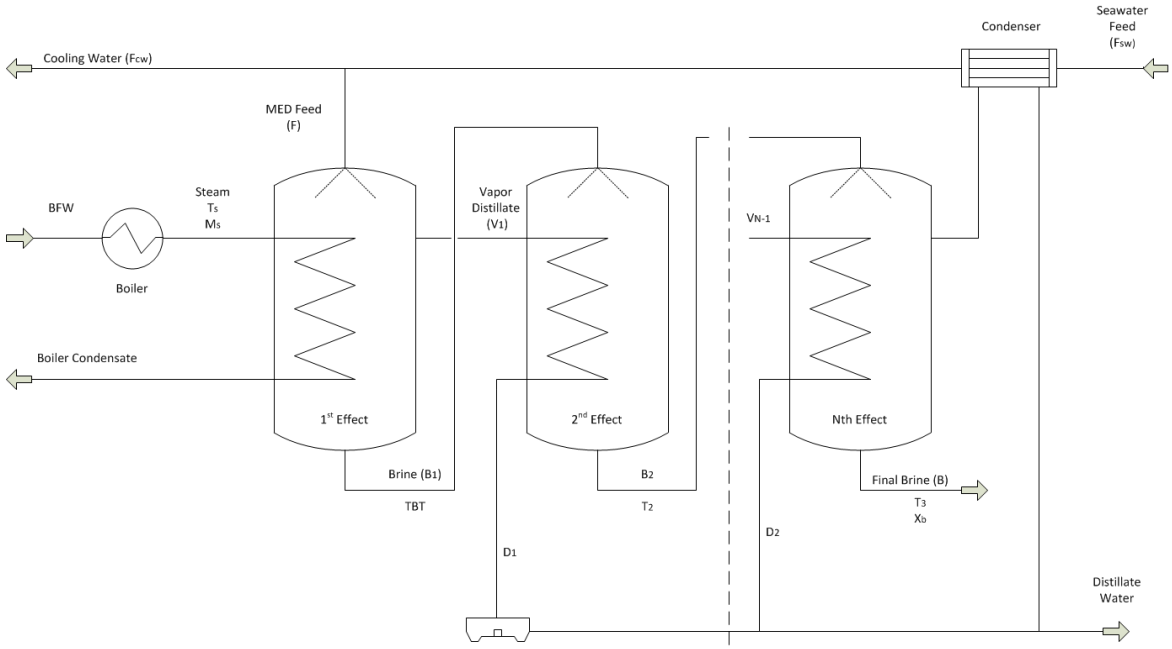

Figure 1. Feed-forward MED desalination schematic

1.2.2 Multi-Stage Flash Distillation (MSF)

Multi-stage flash distillation (MSF) has been the primary thermal technology in desalination. It produces water through the preheating of feed saline water by external sources and then allowing the heated water to flash in consecutive stages. MSF differs from MED in its thermodynamic mechanism to generate water vapor. The primary mechanism for generating water vapor in MSF is flashing at decreasing-pressure stages, while evaporation on the surface of evaporator's tubes is the dominating mechanism in MED. MSF gains two major advantages over MED. First, water generation takes place across the whole water volume allowing for a higher

water production when compared to MED. MED is also more porn to salt scaling on the surface of evaporator's tube. Hence, MED is operating at a lower temperature to overcome the scaling problem. To the contrary to these disadvantages, MED is thermally more efficient than MSF from a thermodynamic aspect (Khawaji, Kutubkhanah, & Wie, 2008).

1.2.3 Membrane Distillation (MD)

Membrane distillation (MD) is an emerging thermal separation process that employs chemical potential difference, essentially vapor pressure difference, between two fluids at different temperatures to drive the mass transfer separation across a hydrophobic membrane. The utilization of a hydrophobic micro-porous membrane reduces the phase separation space required, otherwise, in other thermal separation processes such as conventional evaporators. MD has many other reported advantages over other separation processes including lower operating temperature and higher tolerance to salt concentration and fouling (Alkhudhiri, Darwish, & Hilal, 2012). It has a subtle application in the field of desalination and wastewater treatment as well as the removal of heavy organics and metals (Garcıa-Payo, Izquierdo-Gil, & Fernández-Pineda, 2000).

There are many types of MD, each striving to strike a balance between heat efficiency, water flux, and capital expenditure. Direct contact membrane distillation (DCMD) is the simplest MD design with the least capital expenditure. However, it endures relatively higher heat loss, allegedly as high as 40% (Qtaishat, Matsuura, Kruczek, & Khayet, 2008; Souhaimi & Matsuura, 2011), which increase its operating cost. Air gap membrane distillation (AGMD) employs an air gap between the two fluids to minimize heat losses through conduction. Thus, the air gap adds a layer of mass transfer resistance reducing flux in the system. Vacuum membrane distillation (VMD) eliminates this resistance by introducing a vacuum gap instead of an air gap. This comes

with the drawback of an increase capital and operating expenditure due to the added vacuum system. Other configurations are also proposed, such as filling the air gap with different materials or water, referred as water gap MD (WGMD) or material gap MD (MGMD) (Francis, Ghaffour, Alsaadi, & Amy, 2013).

MD has grasped immense research interest in recent years. The number of research activity on MD has almost doubled in the last decade between 2000 and 2010. The upsurge in MD research in early 1980s was due to breakthroughs in membrane manufacturing that improved the membrane characteristics and performance (Khayet, 2011). It is worth noting that the highest researched configuration in MD is DCMD followed by AGMD and VMD. The focus on DCMD, on the author's opinion, is for researchers to develop a more fundamental understanding of the MD process and the available membrane performance. Hence, DCMD research has been very useful to establish the base for other configurations to evolve. Corroborating the authors prospect is the trend of commercializing MD configurations other than DCMD, such as AGMD in the case of MEMSTILL (Hanemaaijer, 2004) and vacuum enhanced AGMD in the case of MEMSYS (Lange, 2011) .

Despite the heavy research on MD, the technology is, hitherto, economically challenged in the field of water desalination due to its low capital productivity and, costing uncertainty, operational immaturity. Operational immaturity refers to our understanding of the long-term operational performance and fouling of MD (Khayet, 2011). The low capital productivity is due the relatively low flux (Ahmad S Alsaadi, Francis, Amy, & Ghaffour, 2014) which entails high capital expenditure for any reasonable residential or industrial production level. Figure 2 shows schematics of the major configurations of MD.

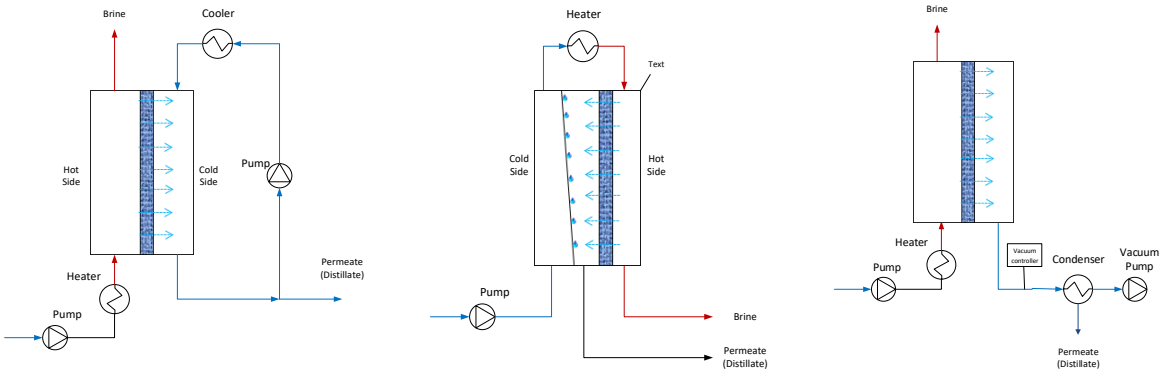

(a) (b) (c)

Figure 2. Configurations of MD (a) direct contact membrane distillation (DCMD) (b) air gas membrane distillation (AGMD) (c) vacuum membrane distillation (VMD)

1.2.4 Integration of Desalination Technologies

The hybridization of emerging desalination technologies is driven by the motive to leverage the advantages of multiple technologies for sustainable design and the betterment of system's economics.

The potential of technological hybridization in water desalination has been elaborated to some extent in the research. MSF-MED integration has been proposed by Dahdah and Mitsos (2014) to tap into the higher thermal efficiency of MED while exploiting the higher temperature tolerance of MSF. MED and reverse osmosis (RO) integration is proposed usually in the context of combined heat and power (CHP) systems for the purpose of adding operational flexibility to the system for efficiency and simultaneous fulfillment of water and power demand (Skiborowski, Mhamdi, Kraemer, & Marquardt, 2012). A bonus in this integration is the increased water recovery in RO due to the higher feed temperature. Ng et al. (2015) recently introduced the integration of MED and AD as a mean to span the operational temperature range in MED, hence, improve the system's throughput. Additionally, ambient heat can be scavenged by the end tail of the system

due to its very low temperature (i.e. 5C). The integration of the emerging Forward osmosis (FO) technology with the conventional reverse osmosis (RO) h been proposed by Bamaga, Yokochi, Zabara, and Babaqi (2011) for the recovery of osmotic pressure, lowering desalination chemical consumption, and reducing fouling and scaling in RO.

1.3 Objectives

The overall objective of the research is to develop a sustainable approach for the synthesis of water desalination systems to fulfill the incessantly increasing water demand through the integration with emerging desalination technologies and exploitation of water-energy nexus opportunities. The objective is achieved through exploring three synthesis problems in water desalination. The specific objectives for each problem are the following:

1. Develop a systematic approach to the optimization of MED-MD seawater desalination system that is thermally coupled with industrial facilities. The proposed approach shall simultaneously optimize the desalination units' design and operating variables as well as the level of energy integration between the industrial process and water desalination.
2. Develop the modelling and design approach for the optimal capacity planning for desalination systems that systematically extracts the optimal process design over time while considering opportunities for heat and mass integration in the system.
3. Design an integrated system for solar-assisted seawater MD desalination and develop the necessary models and approach for the synthesis and scheduling of the system.

CHAPTER II

OPTIMIZATION OF MULTI-EFFECT DISTILLATION WITH BRINE TREATMENT VIA MEMBRANE DISTILLATION AND PROCESS HEAT INTEGRATION[*]

2.1 Introduction

Membrane Distillation (MD) has gained traction in the field of water desalination primarily for its modularity, higher tolerance to salinity, and low-grade-heat utilization. These advantages are useful in the scheme of the integration with conventional desalination such as MED where the brine is treated by MD to improve the system's recovery. In this chapter, an optimization approach to the design of MED-MD integrated system is developed. The system is also thermally integrated with industrial facility while any additional required thermal energy is supplied from external sources.

The optimization framework targets optimizing the operating and design variables of the MED and MD units as well as the excess heat extracted from the industrial facility. At the end of the chapter, a case study is presented at the end of the chapter to illustrate the applicability of the approach.

2.2 Literature Review

Much of the work on membrane distillation (MD) in literature is focused on experimental results and theoretical modeling. The modeling and experimentation work has been expanded recently to MD integration with other desalination technologies such as reverse osmosis (RO) (El-

[*] Reprinted (adapted) with permission from (Bamufleh, H., Abdelhady, F., Baaqeel, H. M., & El-Halwagi, M. M. (2017). Optimization of multi-effect distillation with brine treatment via membrane distillation and process heat integration. Desalination, 408, 110-118). Copyright (2017) Elsevier.

Zanati & El-Khatib, 2007), freeze desalination (FD) (Wang & Chung, 2012), ultrafiltration (UF) (Gryta, Karakulski, & Morawski, 2001), and adsorption desalination (AD) (Shahzad, Ng, Thu, Saha, & Chun, 2014). MED-MD integration has been also investigated experimentally by (De Andres, Doria, Khayet, Pena, & Mengual, 1998) and (Mabrouk, Elhenawy, Mostafa, Shatat, & El-Ghandour, 2016).

On the field of system design and optimization, the focus is to lower the cost of the MD desalination by means of heat integration with excess process heat. The transshipment model has been employed for the targeting of the heat integration of MD with processing facility (Nesreen A Elsayed, Barrufet, & El-Halwagi, 2013). González-Bravo et al. (2015) expands the work by looking at the simultaneous design of the heat exchanger network in an industrial facility and MD system. Gabriel et al. (2016) has developed the optimization framework for the integration of MD across water-energy nexus of industrial processes.

This research stands out from previous research by developing the optimization framework for the synthesis of MED-MD desalination system considering heat integration with an industrial process.

2.3 Problem Statement

Given is an industrial demand of desalinated water of D_{Total}. MED and MD are to be utilized to satisfy the demand supplying MED and MD, respectively. The heat required for desalination can be external or by means of thermal coupling with the industrial facility. The industrial facility has a given number of hot and cold steams with known heat duties, supply temperatures, and target temperatures. The task is to develop an optimization approach to synthesize the desalination system and integrate the desalination system with the processing facility. The optimization variables in each of the subsystems are shown in Table 1.

Table 1. Optimization variables in MED, MD, and industrial process integrated system

MED	MD	Industrial Process
Seawater flowrate to MED and total MED Distillate flowrate	Size of the MD unit (i.e. membrane area)	Excess heat transferred from the industrial facility
Number and size of MED effects	Preheating temperature of the brine entering the MD network	
Flowrate of steam used in the MED system	Distillate flowrate from MD	
Top brine temperature (TBT) of the MED system		

2.4 Approach and Optimization Formulation

The optimization formulation at hand deals with three interlinked subsystem: industrial thermal heat, MED, and MD. The superstructure for the overall system is shown in Figure 3. Superstructure flowsheet for the integrated MED-TMD-industrial process system. First, the methodology to determine the excess heat from the industrial facility is determined (e.g. section 2.5.1). Thermal pinch analysis techniques (El-Halwagi, 2011) can be used for the integration hot and cold streams. Next, the models used for each desalination system is developed (section 2.5.2 & 2.5.3). Finally, the overall optimization approach is presented (section 2.5.4).

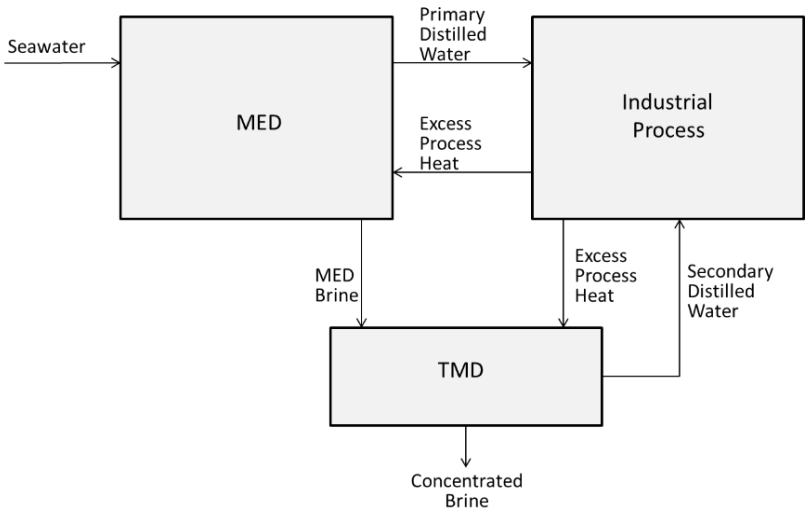

Figure 3. Superstructure flowsheet for the integrated MED-TMD-industrial process system

2.4.1 Thermal Pinch Analysis

External heating and cooling in any industrial process is determined by the level of heat integration within the process streams. Heat integration is the exchange of heat between streams that need to be cooled and streams that need to be heated before the introduction of external utilities for heating and cooling (El-Halwagi, 2017). Proper heat integration results in the reduction of both utilities: hot and cold. The tool used for proper heat integration is called thermal pinch analysis. In thermal pinch analysis, the thermodynamic limits of heat transfer is determined based on the streams quality (i.e. temperature) and quantity of enthalpy. The thermal pinch represents the point where the cold streams (e.g. cold composite curve) extracts the maximum heat from the process hot streams (e.g. hot composite curve). Beyond the thermal pinch, heat transfer is deemed thermodynamically infeasible.

In the design of utility system or cross-process heat integration like the design problem in this chapter, it is more convenient to represent the composite curves in one graph that shows the external hot and cold utilities required at different temperature levels. This curve is called the grand

composite curve. Through the grand composite curve, we are able to determine the quantity of heat available at each temperature level that can be extracted from the industrial process to the desalination system.

2.4.2 MED Model

The modelling of MED presented, hereafter, assumes a feed-forward MED configuration. The number of evaporative effects is denoted as N and given the subscript n. The overall mass balance and component mass balance equations for the first effect is given separately from the remaining effects as it is heated by external heat source. They are shown, respectively, in (1) and (2).

$$F = D_1 + B_1 \tag{1}$$

$$F\ x_F = B_1 x_{B,1} \tag{2}$$

where F, B_1, and D_1 are the flowrates of the seawater feed, 1st effect brine, and 1st effect distillate. x_F and $x_{B,1}$ are the component mass composition of the feed and the 1st effect brine respectively. It is noteworthy that the equations assume a one-component impurity in the seawater feed. Yet, it can be easily expanded to the multi-component case as long as the impurities are inorganic (i.e. the assumption of 100% separation in thermal desalination is valid). Heat balance are given by:

$$F\ h_F = M_s \Delta H_{vw,s} = D_1 H_{D,1} + B_1 h_{B,1} \tag{3}$$

where h_f, $H_{D,1}$, and $h_{B,1}$ are the specific enthalpy for the feed, distillate vapor, and brine in the 1st effect. $\Delta H_{vw,s}$ is the heat of vaporization of the external steam. Similar model equations are developed for the remaining effects shown in (4-6). The subscript n represents the effect number that extends to the total number of effects N.

$$B_{n-1} = D_n + B_n \quad \forall n \tag{4}$$

$$B_{n-1}\, x_{B,n-1} = B_n\, x_{B,n} \quad \forall n \tag{5}$$

$$B_{n-1} h_{B,n-1} + D_{n-1} \Delta H_{vw,D_{n-1}} = D_n H_{D,n} + B_n\, h_{B,n} \quad \forall n \tag{6}$$

The total distillate is the summation of distillate from all effects while the MED brine reject is the last-effect brine flowrate:

$$W_D^{MED} = \sum_{n=1}^{N} D_n \quad \forall n \tag{7}$$

$$W_B^{MED} = B_N \tag{8}$$

where W_D^{MED} and W_B^{MED} is MED total distillate and brine mass flowrates, respectively. The heat transfer area of the effect is estimated by:

$$A_{MED,n} = \frac{Q_{MED,n}}{U_{MED,n}\, \Delta T_{lm,n}} \quad \forall n \tag{9}$$

where $A_{MED,n}$, $Q_{MED,n}$, $U_{MED,n}$, and $\Delta T_{lm,n}$ are the heat transfer area, heat duty, overall heat transfer coefficient, and log mean temperature difference at a specific effect. The heat duty given by (10) and the overall heat transfer coefficient determined from actual data or estimated by empirical equations, (11) as an example (El-Halwagi, 2017).

$$Q_{MED,n} = D_{n-1} \Delta H_{vw,D_{n-1}} \quad \forall n \tag{10}$$

$$U_{MED,n} = 0.8552 + 4.7 * 10^{-3}\, T_{B,n} \quad \forall n \tag{11}$$

A short-cut method for designing MED proposed by (El-Halwagi, 2017) assumes an identical sizing of all effects except for the first evaporative effect. The exception is based on the

fact the first effect is heated by external heat, usually providing significantly higher duty compared to the remaining effects. Additionally, the shortcut method utilizes Gained Output Ratio (GOR) empirical correlation to decouple heat and mass design equations as in (13). Gained output ratio is defined as the ratio of total distillate mass flowrate from the system and the consumed steam mass flowrate as in (12).

$$GOR = \frac{\sum D_n}{M_s} \tag{12}$$

$$GOR = N \cdot (0.98)^N \tag{13}$$

2.4.3 MD Model

Models for MD are generally categorized by the number of space dimensions they cover. Zero-dimensional (0-D) models evaluate heat and mass transfer based on the average conditions over the whole membrane module. On the other extreme, 2-D models (i.e. CFD) evaluates the heat and mass transfer across the 2-dimensional membrane surface and is computationally very expensive (Ahmad Salem Alsaadi et al., 2013). Available MD models assume different level of dimensions. Amongst others, Chernyshov, Meindersma, and de Haan (2003) has established a 2-D model for temperature and salt distribution in MD. Alklaibi and Lior (2005) focused their modeling work on a 2-D transport analysis of MD. For 1-D modeling of MD, two research work stands out by Guijt, Meindersma, Reith, and De Haan (2005) and Ahmad Salem Alsaadi et al. (2013). A Cipollina, Di Sparti, Tamburini, and Micale (2012) has developed a simple 0-D model to evaluate the impact of the geometrical and operating parameters on the unit performance. F. A. Banat and Simandl (1998) developed a model for MD incorporating temperature and concentration polarization alike.

The model equations used for the membrane distillation (MD) subsystem is adopted from (Nesreen A Elsayed et al., 2013). Derived from Fick's law of diffusion, the trans-membrane mass flux is correlated with the water partial pressure difference across the membrane as in (14). Since MD permeate is assumed pure water, the flux equation translates into (15).

$$J_w = K_w \Delta p_w \tag{14}$$

$$J_w = K_w (p^o_{w,f}\, \gamma_{w,f} x_{w,f} - p^o_{w,p}) \tag{15}$$

where J_w is the permeate flux, K_w is the membrane permeability, $p^o_{w,f}$ and $p^o_{w,p}$ are water vapor pressure at the feed and permeate conditions, and $\gamma_{w,f}$ is activity coefficient. The vapor pressure of water at the feed and permeate temperature can be estimated by Antoine equation.

$$p^o_{w,f} = \exp\left(23.1964 - \frac{3816.44}{T_{m,f} - 46.13}\right) \tag{16}$$

$$p^o_{w,p} = \exp\left(23.1964 - \frac{3816.44}{T_{m,p} - 46.13}\right) \tag{17}$$

where $T_{m,f}$ and $T_{m,p}$ are the temperature at the membrane film at the feed and permeate sides, respectively. A suitable correlation can be used for the estimation of the activity coefficient. For example, (18) can be used for the NaCl water solution.

$$\gamma_w = 1 - 0.5\, x_{NaCl} - 10\, x^2_{NaCl} \tag{18}$$

The membrane permeability is another key parameter to determine for the flux estimation. In addition to the characteristics of the membrane such as its porosity, tortuosity, etc, permeability is also a function of temperature. The nature of all these factors with permeability is dependent on the diffusion mechanism dominating the system. (19) and (20) show, respectively, the permeability model for two key diffusion mechanisms: molecular diffusion and Knudsen diffusion.

$$K_w^{mol} = \frac{\pi P D_w r^2}{R p_a \tau \delta} \cdot \frac{1}{T} \tag{19}$$

$$K_w^K = \frac{2\pi\, r^3}{3RT\ \tau\delta} \cdot \left(\frac{8R}{\pi M_w}\right)^{0.5} \tag{20}$$

whereK_w^{mol} and K_w^K are the molecular-diffusion and Knudsen permeability factors, respectively. P is the total pressure inside the membrane pores, D_w is the diffusion coefficient for water in air, r is the pore radius, p_a is air pressure in the pores, τ is the membrane tortuosity, δ is the membrane thickness, M_w is molecular weight of water, and T is the absolute temperature of the membrane.

As illustrated in the previous equations, the mass transfer and heat transfer across the membrane are intertwined. To avoid the complexity of the simultaneous calculations of heat and mass transfer, a correlation of the temperature polarization coefficient is employed to estimate the temperature profile in the membrane, (22). Temperature polarization coefficient (θ) is the ratio of the temperature difference between the two films of the membrane and the temperature difference between the bulk feed and permeate, as in (21).

$$\theta = \frac{T_{m,f} - T_{m,p}}{T_{b,f} - T_{b,p}} \tag{21}$$

$$\theta = \alpha - \beta T_{b,f} \tag{22}$$

where $T_{m,f}$ is temperature of the feed at the membrane, $T_{m,p}$ is the temperature of the permeate at the membrane, $T_{b,f}$ is the temperature of the feed in the bulk, and $T_{b,p}$ is temperature of the permeate in the bulk. α and β are linear correlation parameters. With a known flux, membrane area can be determined for any level of water production by:

$$A_{MD} = \frac{W_D^{MD}}{J_w} \tag{23}$$

where A_{MD} is total membrane area in m^2 and W_D^{MD} is the membrane distillate production. Next, the estimation of heat requirement is done through a thermal balance of the MD subsystem. The term, thermal efficiency ($\eta_{thermal}$) is introduced. It is defined as the ratio of heat used in flux vaporization to the heat provided to the MD system. As the primary source of thermal losses, transmembrane heat conduction is used to estimate thermal efficiency of the system.

$$\eta_{thermal} = 1 - c_{loss} \cdot \eta_{conduction} \tag{24}$$

where c_{loss} is a multiplier constant to estimate the overall heat losses (i.e. conduction, environmental losses, etc.) in respect to conduction losses, and $\eta_{conduction}$ is the conduction heat flux ratio to the overall transmembrane heat flux. The conduction heat flux is derived from Fourier's law of conduction. Hence, thermal losses parameter is given by:

$$\eta_{conduction} = \frac{\frac{k_m}{\delta}\left(T_{m,f} - T_{m,p}\right)}{J_w H_{vw} + \frac{k_m}{\delta}\left(T_{m,f} - T_{m,p}\right)} \tag{25}$$

where k_m and δ are the membrane thermal conductivity and thickness, respectively. Typically, MD brine is recycled for water recovery enhancement. If the recycle stream on the MD is included, the thermal energy balance is adjusted to the following equation:

$$\eta_{thermal}\ (1 + v) \cdot W_f^{MD} c_p \left(T_{b,f} - T_c\right) = W_D^{MD}\ \Delta H_{vw} \tag{26}$$

As shown in the superstructure, MD is fed from the brine of MED system. This is expressed mathematically as follows:

$$W_B^{MED} = W_{reject}^{MED} + W_f^{MD} \tag{27}$$

where W_{reject}^{MED} is MED brine flow that is rejected directly without additional treatment by MD.

2.4.4 Optimization Formulation

The objective function of the problem is the minimization of the total annualized cost given by:

$$TAC = AFC_{MED} + AOC_{MED} + AFC_{MD} + AOC_{MD} \tag{28}$$

where AFC and AOC are the annualized fixed cost and annual operating cost for the subscripted system. The problem is classified as a mixed-integer nonlinear program (MINLP) which is hard to solve globally. Hence, the following systematic approach is proposed to determine the optimal policy of the problem efficiently. Figure 4 shows a flowchart of the proposed optimization approach. The approach is based on Bellman's principle of optimality, which states that the optimal policy of an optimization problem can be reached if constructed efficiently from the optimal solutions of its sub-problems. In this study's problem, the optimal policy is constructed carefully from the solutions of its three sub-problems: industrial thermal system, MED, and MD. For industrial thermal system, thermal pinch analysis technique is utilized to determine the process excess heat quantity and temperature. The diagram is a resultant of maximum heat exchange between the process's hot and cold streams. This is considered part of the optimal policy because it takes the full advantage of the industrial excess heat and simultaneously reduces industrial cooling and desalination heating requirements.

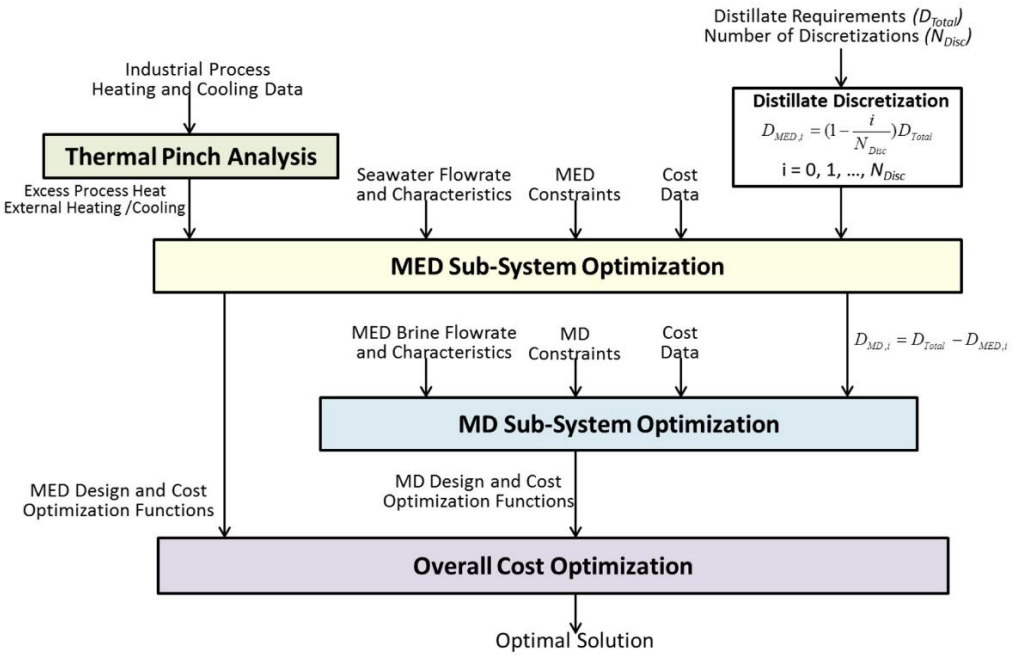

Figure 4. Optimization approach flowchart for the synthesis of MED-MD-industrial process integrated system

Knowing the industrial excess heat to the two desalination systems, we are left with the tedious task of simultaneously optimizing MED and MD design and operating variables. Our approach to solve the highly nonconvex problem is founded on decomposition through discretization technique. The total water demand W_D^{total} is discretized to a heuristically-determined number of discretization points N_{disc}. This number determines the split of total distillate supply between the two desalination systems according to (30).

$$W_D^{Total} = W_D^{MED} + W_D^{MD} \tag{29}$$

$$W_{D,i}^{MED} = \left(1 - \frac{i}{N_{disc}}\right) W_D^{Total} \qquad i = 0,1, \dots, N_{disc} \tag{30}$$

The split is iteratively and discretely changed to determine the water supply from MED system and, subsequently, the remaining water supply comes from MD. At each iteration, the

optimal policy for the operating and design variables for the MED system is determined. That includes the optimum number of effects, the top brine temperature, and the brine conditions. Similarly, MD system is optimized at each iteration to determine the optimum membrane feed temperature, recycle flowrate, and membrane area. As a result, an optimal policy for each subsystem is generated as a function of the discretized distillate flowrate.

2.5 Case Study

It is sought to design an optimized MED-MD desalination system to supply 3,850 tonnes/day of desalinated water to an adjacent industrial facility. The seawater feed has 35,000 ppmw of solute at 298K. Thermal heat can be either from an external utility provided by a fired boiler at 378K at a cost of $1.5 per million kJ or from the thermal coupling with the industrial facility. The hot and cold streams details are provided in Table 2. There exists environmental constraints on the concentration and flowrate of brine of the system detailed in each scenario. The temperature of MED last effect can go as low as 308K limited by the temperature of the cooling water. MED brine from the last effect is limited to 70,000 ppmw. For MD, a polypropylene hollow-fiber membrane MD020CP2N manufactured by Microdyn is used. The hollow fibers have a length, inner diameter, and outer diameter of 0.45 m, 1.5 mm, and 2.8 mm. Remaining details on the membrane can be found in (Al-Obaidani et al., 2008). The membrane maximum temperature limit is 350K.

Table 2. Hot and cold streams available for heat integration (case study #1)

Stream	Heat Capacity Flow (kW/K)	Supply Temperature (K)	Target Temperature (K)
H_1	10	430	410
H_2	126	400	320
H_3	452	390	380
C_1	15	400	450
C_2	165	348	380

The fixed cost functions for the MED and MD are adopted from (El-Halwagi, 2017) and (Nesreen A Elsayed et al., 2013), respectively, and shown below. $A_{EVAP}^{0.6}$ is MED evaporator area in m^2.

$$AFC_{MED} = N \cdot (600\ A_{EVAP}^{0.6}) \tag{31}$$

$$AFC_{MD} = 58.5\ A_{MD} + 1115\ W_D^{MD} \tag{32}$$

For each of the scenarios detailed in Table 3, determine the optimal system design and minimum cost of water.

Table 3. Optimization scenarios for case study #1

Scenario	Pinch analysis limit	Hot utility cost ($/106 kJ)	limit of brine flowrate (kg/s)
1	H_1, H_2, C_1, C_2	1.5	15.5
2	$H_1, H_2, \ C_1, C_2$	1.0	15.5
3	H_1, H_2, C_1, C_2	1.5	37.0
4	H_1, H_2, H_3, C_1, C_2	1.5	15.5

The problem was solved using LINGO software. The results from the base case (e.g. scenario #1), include a 10-effect MED unit coupled with a 3,750 m^2 MD unit for brine treatment. Thermal pinch analysis for the available industrial cold and hot streams is developed in Figure 5. It shows 4800 kW available for heat integration at a starting temperature of 358K. The remaining 13,332 kW is provided by the utility fired heater. The unit cost of water is $1.65 per m^3.

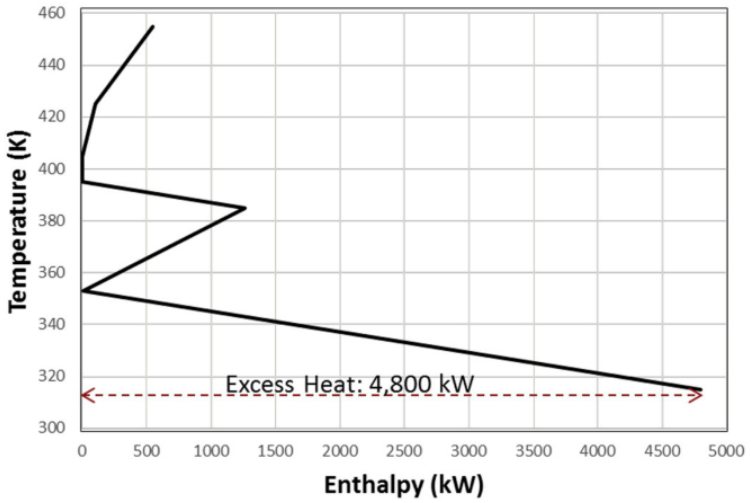

Figure 5. Scenarios #1-3 grand composite curve for industrial facility (case study #1)

When cost steam is reduced as in scenario #2, a reduction in the capital investment of the desalination system is observed. The number of evaporative effects in MED drops from 10 to 8 while the optimum MD area drops to 3,596 m^2. This is a good illustration of the fixed cost-operating cost tradeoff in the system. The unit cost for this scenario is 1.42 per m^3. The optimal solution for scenario #1 and #2 including the system's temperatures are shown in Figure 6 and Figure 7.

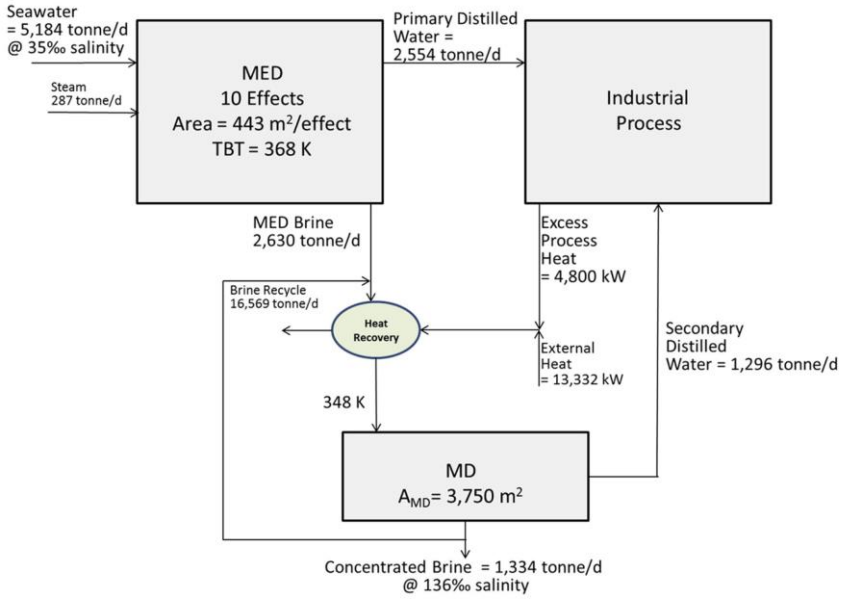

Figure 6. Optimal MED-MD-industrial process flowsheet for scenario #1 (case study #1)

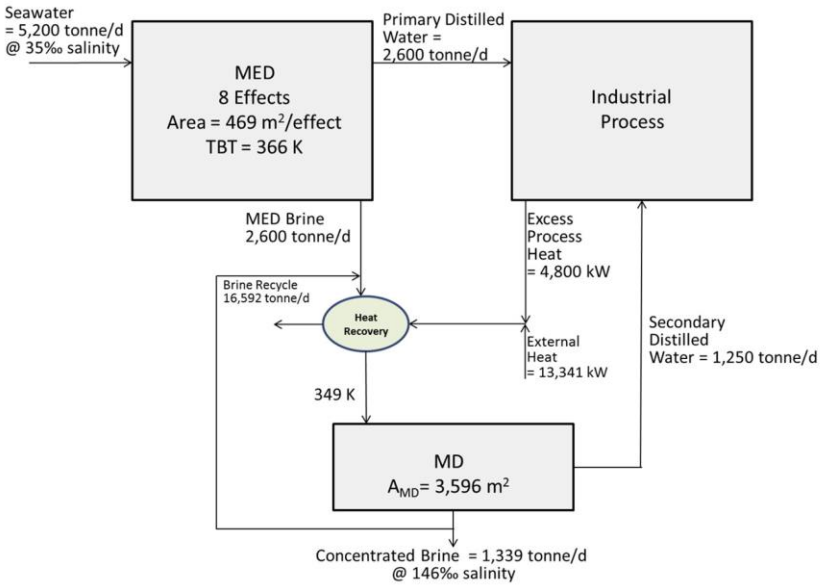

Figure 7. Optimal MED-MD-industrial process flowsheet for scenario #2 (case study #1)

In scenario #3, the brine reject flowrate is relaxed to 37 kg/s. The results are shown in Figure 8 with a unit cost of \$0.61 per m^3. It is important to notice that in the previous two scenarios, MED design was constrained by the brine salinity (i.e. 70,000 ppmw). When the total brine reject of the system was relaxed, the optimization has leveraged the lower cost of MED desalination by an additional brine reject from MED.

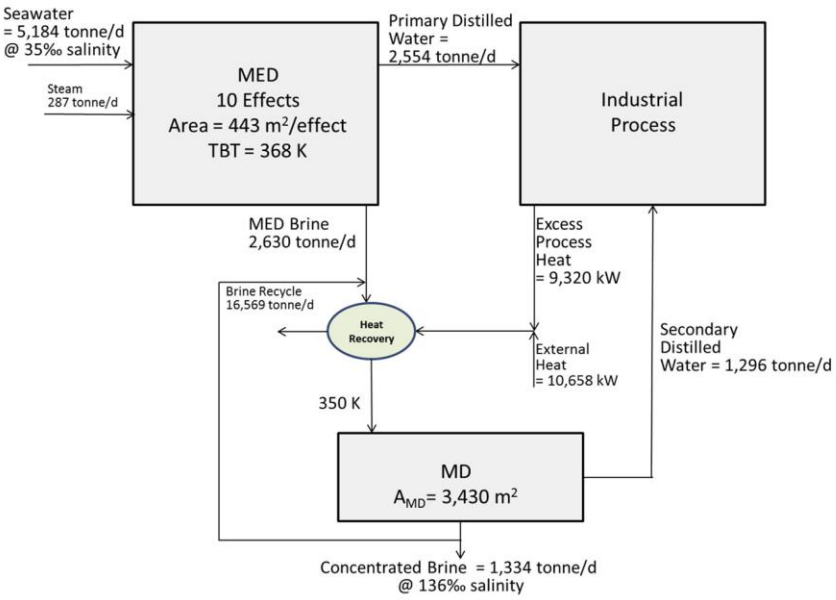

Figure 8. Optimal MED-MD-industrial process flowsheet for scenario #3 (case study #1)

In the final scenario, the pinch analysis is re-evaluated and shown in Figure 9. Available excess heat is now totaling 19,320 kW at two temperature levels (i.e. 375K and 315K). The optimization results shown in Figure 10 make up a unit cost of \$1.55 per m^3.

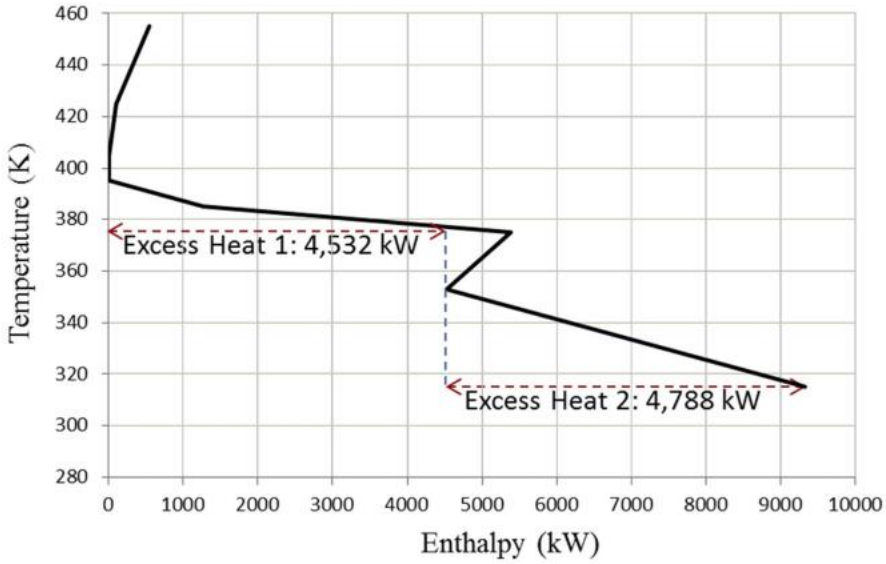

Figure 9. Scenarios #4 grand composite curve for industrial facility (case study #1)

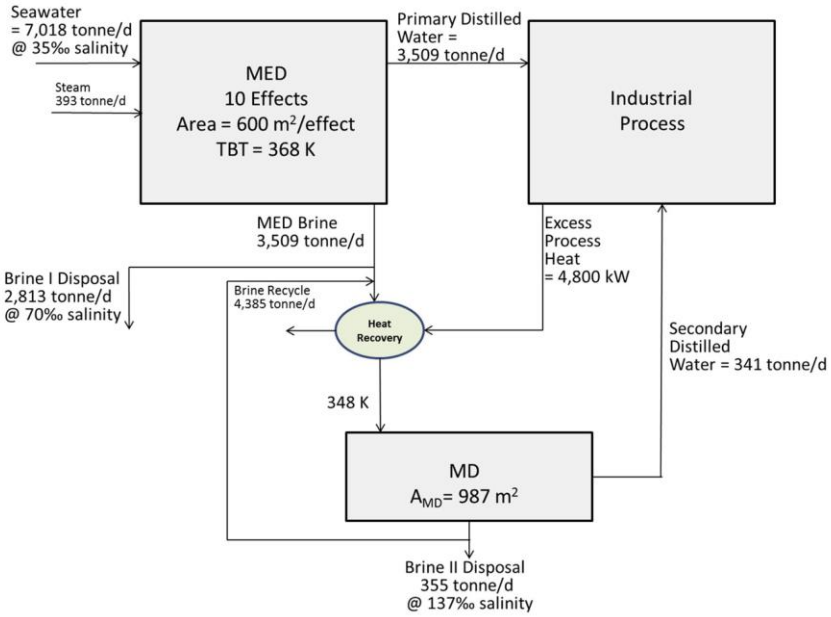

Figure 10. Optimal MED-MD-industrial process flowsheet for scenario #4 (case study #1)

CHAPTER III

OPTIMAL MULTI-SCALE CAPACITY PLANNING IN SEAWATER DESALINATION SYSTEMS[†]

3.1 Introduction

In arid regions of the world, thermal desalination technologies such as multiple effect distillation (MED) are mainstream for producing desalinated water for both residential and industrial sectors. Desalination technologies in general and thermal desalination technologies in specific are generally characterized by their high capital intensity. For example, fixed cost charges in MED typically account for 40-50% of the unit cost of production while it is 30% in RO systems. Examining the capacities of desalination projects in arid areas such as the Gulf countries, one cannot but notice the widespread use of large capacity desalination projects. Large desalination plants were justified in the past to cope with the booming population in the area. For example, the population growth rate in Saudi Arabia has increased incessantly from 3% in 1960 to over 6% in 1982 ("Population Growth Rate: Saudi Arabia," 2017). However, it has plateaued since then at around 2%. Despite that, the trend of installing large desalination projects has continued in recent years. In 2014, Saudi Arabia built one of the world's largest desalination plants with a design capacity of 226 million Imperial gallons per day (MIGD) using multi-stage flash (MSF) and reverse osmosis (RO) (Water-Technology). The country is expected to spend $27 billion in the next 20 years toward desalination projects. Hence, planning for capacity expansion of desalination systems in such situation poses a great multi-period multi-scale optimization opportunity.

[†] Reprinted (adapted) from (Baaqeel, H., & El-Halwagi, M. (2018). Optimal Multiscale Capacity Planning in Seawater Desalination Systems. Processes, 6(6), 68). Creative Commons CC BY 4.0

Large investments are typically justified by the economies of scale associated with large projects and, in some cases, additional technological and operational limitations. However, as many technological and operational limitations diminish with the maturity of desalination technologies, the design capacity of future desalination projects is primarily an economic optimization problem. The downside of large investments lies in the higher fixed operating cost associated with larger underutilized systems and lower capital productivity.

However, with the increasing demands for water and the dwindling resources of fresh water, the conventional approach to the capacity planning problem in distressed desalination systems poses a challenge as the conventional approach of undertaking large expansion projects can lead to low utilization and, hence, low capital productivity. In addition to the option of retrofitting existing desalination units or installing additional grassroots units, there is an opportunity to include emerging modular desalination technologies.

In this chapter, the aim is to develop an optimization framework for the capacity planning in distressed desalination networks considering the integration of conventional plants and emerging modular technologies such as membrane distillation (MD) as a viable option for capacity expansion. The developed framework addresses the multiscale nature of the synthesis problem as unit-specific decision variables are subject to optimization as well as the multi-period capacity planning of the system.

A superstructure representation and optimization formulation are introduced to simultaneously optimize the staging and sizing of desalination units as well as design and operating variables in the desalination network over a planning horizon. Additionally, a special case for multi-period capacity planning in MED desalination systems is presented. A case study is solved to illustrate the usefulness of the proposed approach.

3.2 Literature Review

The optimization of the capacity planning problem has been widely studied from different vistas. In the field of Operational Research, it is studied under the problem formulation of "*Time-Capacity Optimization*." The essence of this field is to optimize the size of future investment, taking advantages of the economies of scale exhibited by larger investments and at the same time minimizing cost associated with money value of time. In a temperas order, Manne (1967) was among the first to develop an analytical solution for the case of constant linear demand growth with an infinite horizon in his book "Investment for Capacity Expansion." Scarato (1969) and explored the time-capacity expansion problem using Manne's framework in urban water systems and MSF desalination systems, respectively. Both studies have contended that the cost function is flat near the optimum point. Other papers have examined the problem in other applications such as in the planning of hydroelectric projects (Hreinsson, 2000), waste treatment systems (Rachford, Scarato, & Tchobanoglous, 1969), and power systems (Billinton & Karki, 2001; Malcolm & Zenios, 1994). The problem was reconstructed by Neebe and Rao (1986) for discrete technologies selection with fixed capacities. Several studies (Iyer & Grossmann, 1998; Maravelias, Sung, & Maravelias; Mitra, Pinto, & Grossmann, 2014; Sahinidis, Grossmann, Fornari, & Chathrathi, 1989) in the field of PSE (e.g. Process Systems Engineering) address the capacity planning optimization for both deterministic and stochastic problems and at various applications and solution techniques.

In water desalination network design, process synthesis techniques have been employed for the design of desalination units of a specific technology. Example research in the synthesis of reverse osmosis networks includes the work by El-Halwagi (1992) and subsequent research contributions (Khor, Foo, El-Halwagi, Tan, & Shah, 2011; Vince, Marechal, Aoustin, & Bréant,

2008). Design and optimization techniques have been developed to assess several configurations of MSF systems for various criteria. Druetta, Aguirre, and Mussati (2014) evaluated the detailed design of MED seawater desalination system for the minimization of total cost where MINLP model is employed to determine the nominal optimal sizing of system's equipment. Gabriel, Linke, and El-Halwagi (2015) used linearization techniques to achieve global solutions of the design of MED systems. Several research contributions have been made in the area of optimizing the synthesis of MD networks for various applications (Nesreen A Elsayed, Barrufet, & El-Halwagi, 2015; Nesreen A Elsayed, Barrufet, Eljack, & El-Halwagi, 2015; González-Bravo et al., 2015). Other research has focused on the synthesis of hybrid desalination systems. Bamufleh, Abdelhady, Baaqeel, and El-Halwagi (2017) developed the framework for synthesis of MED-MD desalination system that is thermally coupled with industrial process. Al-Aboosi and El-Halwagi (2018) developed an approach for the optimization of the design of RO-MED hybrid systems using a water-energy nexus approach. Huang et al. integrated multiple desalination technologies with combined heat and power in industrial and power plants (Mapunda, Chen, & Yu, 2018). Kermani, Kantor, and Maréchal (2018) provided a review of water-heat nexus with a meta-analysis of network features.

Notwithstanding previous research in the field, to the extent of the authors' knowledge, no optimization framework has been established for the multiscale optimization of capacity planning in water desalination systems taking into consideration mass and heat integration opportunities with emerging desalination technologies. This paper aims at developing an optimization formulation for the capacity expansion planning that systematically extracts the optimal process design over time from numerous alternatives while considering retrofit options of existing desalination units and heat and mass integration between desalination systems. It will also

simultaneously optimize the intra-process design and operating variables. This work seeks to answer the following questions in the context of capacity planning of desalination systems:

- What is the optimum staging/sizing of the new desalination units that optimize the selected objective function? Which technologies should be selected for water demand satisfaction?
- What are the optimum design and operating variables (i.e. evaporator's area, top brine temperature, etc.) for the existing and newly installed desalination units over the planning horizon?
- How shall existing and new desalination units in each planning interval be integrated (i.e. mass and heat integration) for the optimization of the objective function?

3.3 Problem Statement

The multi-scale capacity planning problem in desalination network may be stated as follows: Given is a water desalination system subject to capacity expansions within a planning horizon of N_t years. The horizon is discretized to annual counterparts, $INTERVAL = (t \mid t = 1, 2, \dots, N_t)$, where $t = 1$ represents the initial time of the planning horizon, satisfied by the initial desalination system. Expansion projects commence at $t = 2$. In each interval, the total water desalination capacity of the system is denoted D_t while the water demand at a given period is denoted d_t. Desalinated water price, Pr_t, may vary in each interval.

The set $CONFIG = (i|i = 1,2, \dots, N_i)$ of desalination configurations are considered to meet the water demand increase. Two subsets for each configuration exist. The set $INLET_i = (m|m = 1,2,..,N_{m_i})$ represents the inlet nodes for i^{th} configuration. The set $OUTLET_i = (n|n =$

$1,2,..,N_{n_i}$) represents the outlet node for i^{th} configuration. For example, the configuration of MED-RO desalination depicted in Figure 11a has two inlet nodes and four outlet nodes, while the one depicted in Figure 11b has one inlet node and three outlet nodes.

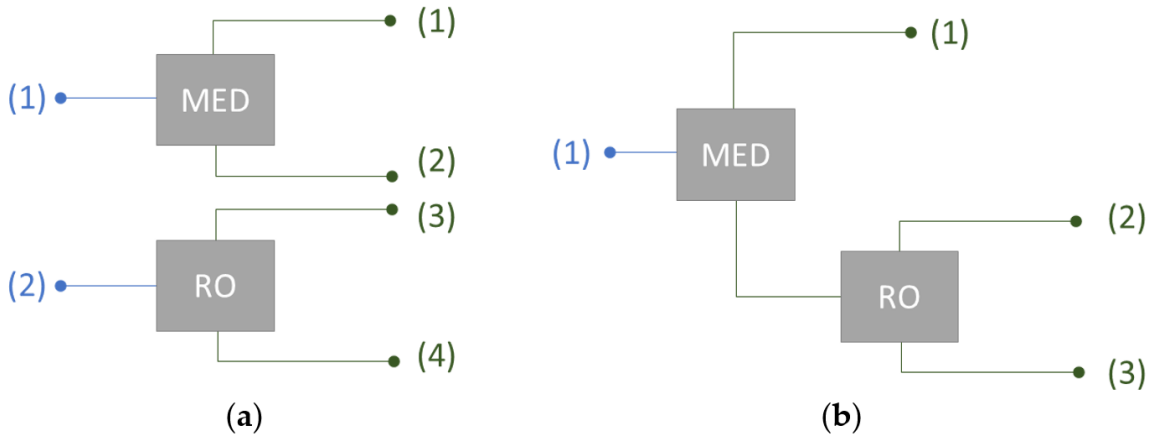

Figure 11. Example configurations for water desalination. (a) with two inlet nodes and four outlet nodes (b) with one inlet node and three outlet nodes

The initial design of the system is fixed with a known distillate capacity of $D_t = D_1$. Due to distillate demand growth in the horizon, expansion of the desalination system is required to meet the planning horizon water demand. Saline water feed, F_t^{sw} with a fixed salinity x^{sw} is available as a feedstock to new desalination units. On the overall system's level, a constraint exists on the total brine reject flowrate B_{max}^{reject} from the system while the salinity of the system's brine and distillate are constrained by x_{max}^{b} and x_{max}^{d}, respectively.

In the context of this study, the objective is to maximize the net present value (NPV) of capital investment portfolio in the system accounting for annual revenue, fixed and operating cost, and book values. However, the formulation may be adjusted to target other objectives such as other

economic, environmental, and reliability objectives. At a given minimum rate on investment (r), the objective is to determine the optimal planning for the desalination system capacity that maximizes the total net present value (NPV) while fulfilling water-demand forecast.

Figure 12 is a schematic representation of the multi-period capacity planning problem in a desalination system. The superstructure shows the multi-period interactions between the potential configurations in each interval.

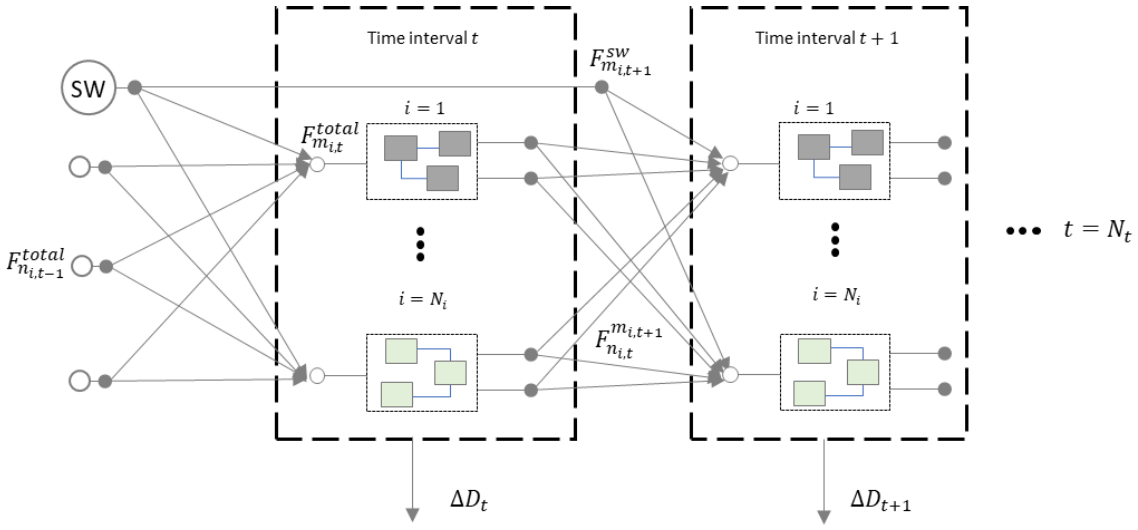

Figure 12. Multi-period superstructure of the desalination capacity planning problem

3.4 Synthesis Approach

The representation in Figure 12 typifies the synthesis approach for the system. The change in the system's distillate capacity is measured by the added capacity at each interval, ΔD_t. It is assumed that the inherited system design from a preceding interval is fixed and changes in the system are limited to the selected configuration added at the current interval and its design variables. Nonetheless, all intervals' designs will be solved simultaneously. In each interval all

possible configurations are evaluated, each named a $SUBSYSTEM_{i,t}$. For example, the first configuration in the second interval holds the notation $SUBSYSTEM_{1,2}$.

The multi-period superstructure is rich enough to embed many potential designs of interest in the desalination system. For example, hybridization of desalination configurations can be done across intervals. However, the complexity of the superstructure can be prohibitive for a feasible mathematical optimization. For example, there is a total of 9,765,625 possible designs for a 10-interval horizon and 5 considered desalination configurations.

Our approach for a feasible optimization is shown in Figure 13. A pre-optimization screening of configurations is carried out on the system. The extensive list of desalination configurations is screened based on characteristic data of the system and knowledge on the commerciality, maturity, and economic efficacy of each configuration. In this step, unfeasible configurations, either economically or technically, based on parameters such as feed water salinity, distillate quality, range of distillate capacity, and minimum required recovery are, first, identified. The pre-optimization screening can be done in one of two ways:

- Complete elimination of configurations as a possible element of the optimal policy. This is applied on configurations with no hope to make it in the optimal flowsheet of the water system. For example, previous research and experience indicates the efficacy of RO in desalinating low- and medium-salinity water feed (i.e. brackish water) compared to MED. However, reliability and performance issues hinder its application for high-salinity water desalination. Hence, knowledge of the system's feed water quality enables the elimination of some desalination technologies and configurations. Other factors for the screening of candidate configurations are listed in Figure 13 that include, but not limited to, their ability to achieve product's quality

(i.e. boron separation), meet a system's constraint (i.e. brine salinity), and achieve an acceptable level of commerciality.

- Disjunction of configuration's selection based on the problem's parameters. For example, the selection between simple MED and MD desalination configurations can be modelled by a disjunctive inequality based on the targeted design capacity, (33). Assuming previous knowledge on the technical and economical feasible capacity range for each configuration, the disjunction can be reformulated using common disjunctive inequality solution techniques such as Convex Hall or Big-M reformulation.

$$\begin{bmatrix} y_{MD} \\ D_{MD}^{min} \leq D_{subsystem} \leq D_{MD}^{max} \\ \vdots \end{bmatrix} \vee \begin{bmatrix} y_{MED} \\ D_{MED}^{min} \leq D_{subsystem} \leq D_{MED}^{max} \\ \vdots \end{bmatrix} \tag{33}$$

Next, key intra-process design variables are screened. Candidate design variables for the application of Bellman's principle of optimality are locally optimized within the configuration. In the cases where the design variable's optimality depends on the design capacity of the potential desalination configuration, a profile of the design variable's optimal policy with the design capacity is developed. The outputs from the disjunction, configurations' modelling, and intra-process design variables optimization are entered into the overall system optimization model. In the next section, the general formulation of the problem is presented, followed by a discussion on the special case of optimizing multiple effect distillation (MED) desalination systems.

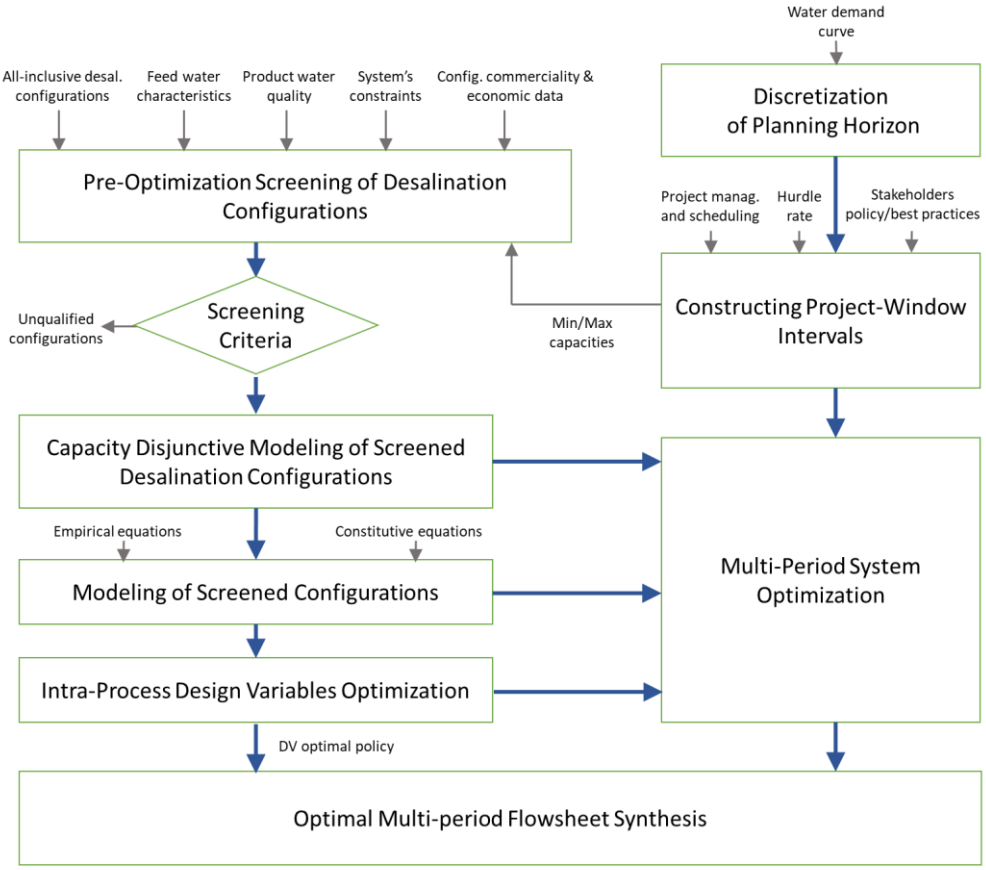

Figure 13. Optimization approach for the multi-period capacity planning problem

3.5 General Formulation

The objective function, presented later in the formulation, is subject to the following constraints:

3.5.1 System's Distillate Capacity

The capacity of the system shall meet or exceed water demand at any t^{th} interval, as expressed in (34), where D_t is the interval system total capacity, and d_t is the interval's water demand.

$$D_t \geq d_t \quad \forall t \tag{34}$$

The total distillate capacity can change across the multi-period horizon. The total system's capacity at a given interval is the summation of the total distillate capacity from the previous interval and the added distillate capacity, ΔD_t, at the interval, as given by:

$$D_t = D_{t-1} + \Delta D_t \quad \forall t \tag{35}$$

The added capacity at any interval consists of the distillate capacity of the subsystems, $D_{i,t}$, installed in the interval.

$$\Delta D_t = \sum_i D_{i,t} \quad \forall t \tag{36}$$

3.5.2 Subsystem's Mass Balance

The mass balance on each subsystem (i.e. configuration) is given by:

$$\sum_m F_{m_{i,t}}^{total} - \sum_n F_{n_{i,t}}^{total} - D_{i,t} = 0 \quad \forall t \; \forall i \tag{37}$$

where $F_{m_{i,t}}^{total}$ is the mass flowrate to the m^{th} inlet node of a given subsystem. The mass flowrates in all inlet nodes constitute the total inlet feed to the subsystem. Conversely, $F_{n_{i,t}}^{total}$ is the mass flowrate for the n^{th} outlet node of the subsystem. The mass flowrates in all outlet nodes from all subsystems constitute the interval's brine reject, as in (39)here $B_{i,t}$ and B_t are the brine flowrate of a subsystem and the interval, respectively.

$$B_{i,t} = \sum_n F_{n_{i,t}}^{total} \quad \forall t \; \forall i \tag{38}$$

$$B_t = \sum_i B_{i,t} \quad \forall t \; \forall i \tag{39}$$

3.5.3 Subsystem's Inlet and Outlet Nodes

Given $F_{n_{i,t}}^{m_{i,t+1}}$ denotes the flow from n^{th} node in $SUBYSYSTEM_{i,t}$ to the m^{th} inlet node in $SUBYSYSTEM_{i,t+1}$, the split of n^{th} outlet node is modelled as follows:

$$F_{n_{i,t}}^{total} = \sum_m F_{n_{i,\mathrm{t}}}^{m_{i,t+1}} \quad \forall t \; \forall i \tag{40}$$

The mixing in m^{th} inlet node in any subsystem is given by:

$$F_{m_{i,t}}^{total} = F_{m_{i,t}}^{sw} + \sum_n F_{n_{i,t-1}}^{m_{i,t}} \quad \forall t \; \forall i \tag{41}$$

where $F_{m_{i,t}}^{sw}$ is the salt water (i.e. seawater) mass flowrate to the inlet node. Similar (35) for distillate capacity, the total seawater flowrate may be represented as the increase of the seawater consumption at a given interval added to the seawater consumption at the previous interval:

$$F_t^{sw} = F_{t-1}^{sw} + \sum_m F_{m_{i,t}}^{sw} \quad \forall t \; \forall i \tag{42}$$

3.5.4 Subsystem's Modeling Equations and Constraints

Each desalination configuration is described by a distinct vector of modelling equations and constraints that characterize the performance and limitations of the subsystems employing the configuration. In addition to the design capacity and compositions, a configuration is characterized by the vectors $DV_{i,t}$ for design variables, $OV_{i,t}$ for operational variables, and $SV_{i,t}$ for state variables.

$$\phi_i\left(D_{i,t}, x_{i,t}^d, x_{i,t}^b, DV_{i,t}, OV_{i,t}, SV_{i,t}\right) = 0 \;\; \forall t \; \forall i \tag{43}$$

$$\phi_i\left(D_{i,t}, x_{i,t}^d, x_{i,t}^b, DV_{i,t}, OV_{i,t}, SV_{i,t}\right) \geq 0 \;\; \forall t \; \forall i \tag{44}$$

Key constraints for desalination configurations include the design capacity as in (45), and limits on some design variables (i.e. membrane area), as in (46).

$$D_i^{min} \leq D_{i,t} \leq D_i^{max} \;\; \forall t \; \forall i \tag{45}$$

$$DV_i^{min} \leq DV_{i,t} \leq DV_i^{max} \;\; \forall t \; \forall i \tag{46}$$

In some cases, the limitation on the design variable extends across intervals. For example, the maximum RO modules in series, or a constraint on the maximum number of evaporative effects in series across all intervals. Such constraints may be captured by the following:

$$\sum_t DV_{i,t} \leq DV_i^{max} \;\; \forall t \; \forall i \tag{47}$$

One key constraint for the system, to be met in all intervals, is the salinity constraint in both the brine and distillate. The following provide the component mass balances for the system's distillate and brine, respectively:

$$x_t^d \cdot D_t = x_{t-1}^d \cdot D_{t-1} + \sum_i x_i^d \cdot \Delta D_t \;\; \forall t \; \forall i \tag{48}$$

$$x_t^b \cdot B_t = \sum_i x_i^b \cdot B_{i,t} \;\; \forall t \; \forall i \tag{49}$$

Given a fixed maximum salinity on the brine, x_{max}^b and the distillate x_{max}^d, the respective constraints is given by:

$$x_t^b \leq x_{max}^b \quad \forall t \tag{50}$$

$$x_t^d \leq x_{max}^d \quad \forall t \tag{51}$$

3.5.5 System's Costing & Objective Function

Total capital investment of each subsystem is correlated with the design variables and design capacity. Total operating cost correlates with the actual distillate production at the interval, as well as, all design and operating variables of the constituent subsystems.

$$TCI_{i,t} = f_i^c\left(D_{i,t}, DV_{i,t}\right) \quad \forall i \; \forall t \tag{52}$$

$$TCI_t = \sum_i TCI_{i,t} \quad \forall i \; \forall t \tag{53}$$

$$AOC_t = f_i^o\left(d_t, DV_{i,t}, OV_{i,t}\right) \quad \forall i \; \forall t \tag{54}$$

The proposed objective function is the maximization of the net present value (NPV) as an economic metric of the desalination system as given by (55). Thus, other economic metrics such as internal rate of return (IRR) may easily be used instead. The terms V_t , AOC_t , and TCI_t represents the revenue, annual operating cost, and total capital investment at t^{th} interval, respectively. All cash flows are properly discounted with the underlying assumption of the cash flow's realization at the beginning of the year. A linear depreciation model with no salvage value is assumed to estimate the system's book value, BV_t, at the end of the planning horizon. The service life, SL, is assumed constant for all units in the desalination system.

$$Maximize \quad NPV = \sum_t \frac{REV_t - AOC_t - TCI_t}{(1+r)^{(t-2)}} + \frac{BV_t}{(1+r)^{(H-1)}} \quad \forall t \tag{55}$$

$$BV_t = TCI_t \cdot \arg max\left(0, 1 - \frac{N_t - (t-1)}{SL}\right) \quad \forall t \tag{56}$$

$$REV_t = d_t \cdot Pr_t \quad \forall t \tag{57}$$

To model the project-window intervals stipulated in synthesis approach, a new constraint is introduced on the allowable intervals for plant's installation. It is unlikely for capacity expansion projects to sequence in annual or biannual basis for economic and other considerations (i.e. safety, reliability, project management, etc.). Assuming a fixed period between project windows, τ, the constraint is enforced by assuming zero added desalination capacity for potential desalination plants in between project-permissible intervals, as given by:

$$\Delta D_t = 0 \quad \forall t \in INTERVAL:\ t \neq \tau, 2\tau, \dots, n\tau \tag{58}$$

3.6 MED Special Case Formulation

Characterized by large design capacity and its capacity for integration with other desalination technologies, seawater Multiple Effect Distillation (MED) desalination systems are good candidates for the presented optimization formulation. In this section, a shortcut method is proposed for the modelling and optimization of capacity expansion planning in MED desalination system. A set of three technologies are considered as modifications in the network to meet water demand. The conventional option is installing a new grassroots MED unit. Alternatively, existing MED units may be retrofitted with additional evaporative effects for additional water recovery or integrated with MD for brine treatment.

Next, a step-by-step application of the synthesis approach in Figure 13 on MED desalination systems for capacity expansion is carried out to develop a shortcut method for the special case.

3.6.1 Desalination Configuration Screening

A strategy of screening unfeasible desalination technologies and technologies that do not integrate with the existing system is adopted. MED and MD are the two technologies considered, forming three distinct configurations: new standalone MED unit, new evaporative effects to existing MED units, and MD unit for brine treatment. MD desalination of seawater is eliminated based on previous techno-economic analysis and research on MD (Bamufleh et al., 2017).

3.6.2 Capacity Disjunctive Modeling

In this step, the search space for the optimal flowsheet is reduced by applying the predetermined knowledge on the optimality of each screened configuration. For the retrofit configuration (EE), a capacity range, D_{EE}^{low} and D_{EE}^{high} is determined in which retrofit is part of the optimality policy. The decision is based on three distinct features of this configuration: limited distillate production, higher energy efficiency, and modest capital investment. The disjunction is expressed mathematically as follows:

$$I_{EE,t}\, D_{EE}^{low} \leq D_t \leq I_{EE,t}\, D_{EE}^{high} \quad \forall t \tag{59}$$

$$I_{EE,t}\, D_{EE}^{high} \leq D_t \leq I_{EE,t}\, D_{MED}^{max} \quad \forall t \tag{60}$$

where $I_{i,t}$ is a binary variable for each desalination subsystem. In the case of one configuration is allowed in each interval, the sum of the binary variables at any given interval must not exceed one.

$$\sum_{i} I_{i,t} \leq 1 \quad \forall t \; \forall i \tag{61}$$

3.6.3 Configuration's Modeling

Various models were evaluated for use in the special formulation for the MED configuration (H. El-Dessouky, Alatiqi, Bingulac, & Ettouney, 1998; El-Halwagi, 2017; Mistry, Antar, & Lienhard V, 2013). A modified version of the MED model presented by (El-Halwagi, 2017) is used here. The modification intends to make the model suitable for capacity expansion optimization applications, in which retrofitting the system with additional effects is considered. All the above mathematical models target a grassroots design. Hence, the implication of adding additional effects on an existing MED unit on water production, steam consumption, and capital and operating cost are not easily inferred. For a given MED system with a variable number of effects, N_{eff}, the total MED distillate production is given by:

$$D_{MED} = \sum_{n=1}^{N_{eff}} D_n \tag{62}$$

where n is the evaporative effect number. D is the distillate water mass flowrate. The heat load of each evaporator, $Q_{evp,n}$ is estimated by the heat of vaporization, λ_n, at the temperature of the evaporator:

$$Q_{evp,n} = \lambda_n \cdot D_n \tag{63}$$

Several types of evaporators may be used including falling film, rising film, and forced circulation. Assuming a horizontal-tube falling film evaporator (HTFFE), the evaporator's design (i.e. area) is given by:

$$Q_{evp,n} = U_{HTFFE,n} \cdot A_{HTFFE,n} \cdot \Delta T_{LM,n} \quad (64)$$

For a conceptual design of a water system like the one treated in this paper, the following simplifying assumption are deemed acceptable, reducing the MED distillate capacity equation to (67):

- The log-mean temperature difference may be assumed equal to the temperature difference between the vapor temperature in the tubes and the evaporator's temperature as in (65).
- The temperature difference between all effects is equal. Therefore, the MED temperature profile is estimated by (66).
- All evaporators are identical in size.

$$\Delta T_{LM,n} = T_{n-1} - T_n \quad (65)$$

$$\Delta T_{LM,n} = \frac{(T_s - T_c)}{N_{eff} + 1} \quad (66)$$

$$D_{MED} = \frac{A_{HTFFE} \cdot (T_s - T_c)}{(N_{eff} + 1)} \sum_{n}^{N_{eff}} \frac{U_{HTFFE,n}}{\lambda_n} \quad (67)$$

Several correlations exist for U_{HTFFE} and λ with temperature, example of which is presented in (68) and (69).

$$U_{HTFFE,n} = 0.8552 \ + \ 0.0047 * T_n \quad (68)$$

$$\lambda_n = -2.7532\, T_n + \ 3278.8 \quad (69)$$

Assuming a linear correlation of both parameters with temperature, the summation term of the U/λ ratio may be correlated to three design variables: Ts, Tc, and Neff. Numerical analysis of the term

shows a linear correlation of the term with N_{eff} at a fixed T_s and T_c values. Therefore, (67) can be rewritten as:

$$D_{MED} = \frac{A_{HTFFE} \cdot (T_s - T_c)}{(N_{eff} + 1)} \cdot (\alpha_{MED} \cdot N_{eff}) \tag{70}$$

α_{MED} is a design parameter, estimated from the steam and cooling water temperature available at the facility. It is linearly estimated by (71), where $a_s \; and \; a_c$ are two scalar values.

$$\alpha_{MED} = \alpha_s \cdot T_s + \alpha_c \cdot T_c \tag{71}$$

Hence, (70) may be rewritten as follows:

$$D_{MED} = \alpha_{MED} \cdot (T_s - T_c) \left(\frac{N_{eff}}{N_{eff} + 1} \right) \cdot A_{HTTFE} \tag{72}$$

The new equation correlates conveniently the unit's total water production with the area and number of evaporative effects. Gained output ratio, GOR, is a useful estimate of the unit's thermal efficiency. It is defined by (73) and empirically estimated by (74).

$$M^s = \frac{D}{GOR} \tag{73}$$

$$GOR = N_{eff}(0.98)^{N_{eff}} \tag{74}$$

Combining (71), (72), and (73), the total steam consumption is given by:

$$M^s = \frac{\alpha_{MED} \cdot (T_s - T_c) \cdot A_{HTTFE}}{(N_{eff} + 1)(0.98)^{N_{eff}}} \tag{75}$$

It is reckoned that (72) and (75) are very useful in modeling the second configuration, the evaporative effects retrofit (EE). Figure 14 shows the distillate capacity and steam consumption

incremental change with the increase or decrease of an evaporative effect, based on the above model.

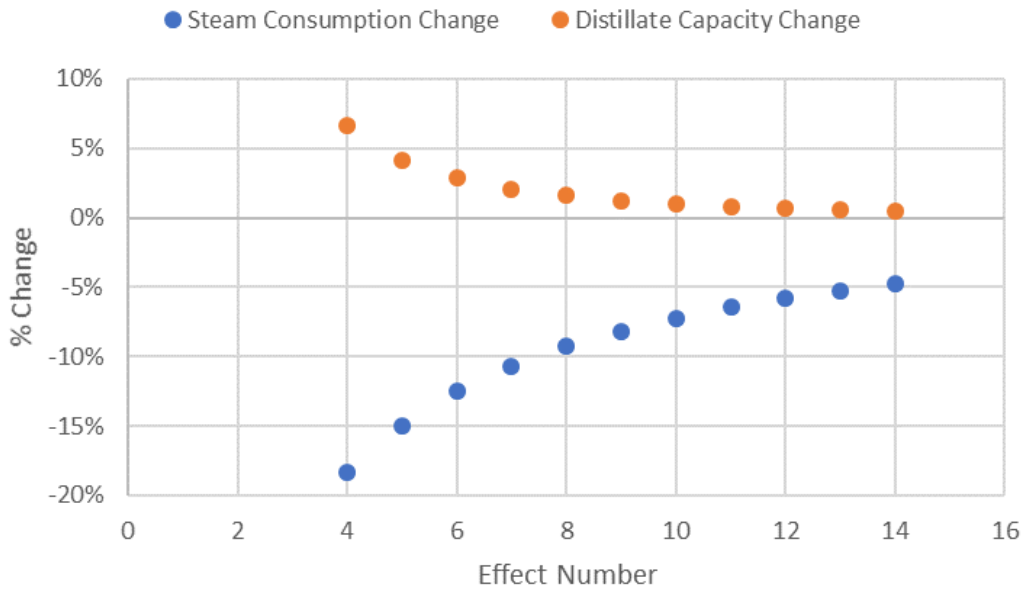

Figure 14. Net change in distillate production and steam consumption with the number of evaporation effects

3.6.4 Intra-Process Design Variables Optimization

In the special case, three design variables within the considered configurations are investigated: top brine temperature (TBT) in MED, number of effects in MED, and bulk feed temperature (TBF) in MD. The optimization TBT and TBF variables are associated with a tradeoff between operating and capital cost in their respective units and have no association with the inter-process design of the system (i.e. subsystem capacity). Therefore, they are locally optimized and inferred as a constituent of the global optimization solution.

The optimization of MED number of effects is, on the other hand, subjective the subsystem's capacity, and must be solved simultaneously with the multi-period planning optimization. Alternatively, an optimal policy of the effect's number and the subsystem capacity is generated and fed to the system multi-period optimization.

3.7 Case Study

3.7.1 Case Study Description

The case study considers the capacity planning of an industrial water desalination system with five identical MED units, each consisting of 6 evaporative effects capable of producing 300 kg/s of distilled water. All the units are currently fully exhausted by the water demand. Due to a planned expansion in the industrial facility, water demand in a horizon of 30 years is expected to drastically increase in the next 20 years, followed by slim increases in the remaining 10 years. The demand curve is shown in Figure 15.

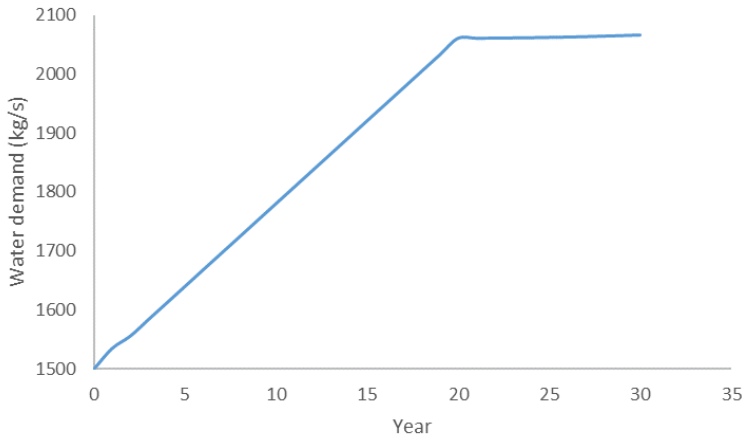

Figure 15. 30-year water demand curve (case study #2)

Seawater feed and brine parameters as well as cost parameters are shown in Table 4. The price of water product is fixed throughout the planning period at \$1.5 per m^3. Project windows are assigned every 5 years (i.e. $\tau = 5$).

Table 4. Design basis for case study #2

Parameter	**Symbol**	**Value**	**Unit**
Seawater feed temperature	T_{sw}	298	K
Seawater salinity	x^{sw}	30,000	ppm
MED brine maximum salinity	x^{b}_{MED}	75,000	ppm
Steam temperature	T_s	373	K
Cooling water temperature	T_c	298	K
Steam price	c_{HU}	2.5	\$/MJ
MED minimum capacity	D^{min}_{MED}	50	kg/s
MED maximum capacity	D^{max}_{MED}	350	kg/s

For MD, a polypropylene hollow-fiber membrane MD020CP2N manufactured by Microdyn is used. The hollow fibers have a length, inner diameter, and outer diameter of 0.45 m, 1.5 mm, and 2.8 mm. Remaining details on the membrane can be found in (Al-Obaidani et al., 2008). MD design and costing model was adopted from (Nesreen A Elsayed et al., 2013). For this case study, membrane permeability, B_w, is assumed constant at $1.92 \times 10^{-7} \frac{kg}{m^2 \cdot s \cdot Pa}$. Annualized fixed cost and annual operating cost for MD system is given by (Al-Obaidani et al., 2008):

$$TCI_{MD} = 459\, A_m + 13{,}117\, (1+\gamma)\, F_{MD} \tag{76}$$

$$AOC_{MD} = c_{HU} \cdot \left(\frac{J_w\, H_{vw}}{\eta_m}\right) + \left(1411 + 43(1-\xi) + 1613(1+\gamma)\right)F_{MD} \quad (77)$$

where c_{HU} is cost of heating utility, ξ is water recovery, γ is ratio of MD recycle flowrate to feed flowrate. Design and costing equations for MED are adopted from (El-Halwagi, 2017). Assuming a Lang-factor of 3.5, the total capital cost is given by:

$$TCI_{MED} = 24{,}600 \cdot N_{eff}\, A_{HTFFE}^{0.6} \quad (78)$$

It is desired to synthesis the expansion of the system for the planning horizon of 30 years, considering the three desalination configurations listed for the MED special case. The objective is to develop an optimal investment strategy to maximize net present value of the system. A minimum rate on investment for stakeholders is 15% (e.g. hurdle rate). In scenario #2, an environmentally-driven limitation of 3,600 $\frac{m^3}{hr}$ on the seawater mass flowrate is considered.

3.7.2 Case Study Solution

The horizon was discretized to annual intervals, $N_t = 30$, with allowable expansion windows every 5 years. The optimization formulations are solved using the software LINGO® (Schrage, 2006). The problem is formulated as MINLP with 1,337 variables and solved on Intel Core i7-6700 CPU with 16GB RAM in 274 seconds. A summary of the optimization results for all the scenarios are shown in Table 5.

Table 5. Results of case study #2

	Units	Base case	Scenario #1	Scenario #2
NPV	$10^6\ \$/year$	-7.1	10.5	6.9
New MED Units (MED)		1	3	3
Retrofitted effects (EE)		0	1	1
Total MD area (MD)	m^2	0	0	10,800
MED top brine temperature	$°K$	358	358	358
MD feed temperature	$°K$	363	363	363

First, two intra-process design variables are optimized locally: the TBT and TBF temperature. Within specific design limits, both involve a tradeoff between capital and operating cost. Higher top brine temperature in MED, for example, yields higher thermal efficiency, (i.e. lower specific latent heat of vaporization) and lower specific evaporative area (i.e. higher heat transfer coefficient). On the other hand, higher unit cost of steam as well as reliability and operability issues (i.e. scaling) may be incurred. The optimum TBT and TBF temperatures for all the scenarios are 358K and 363K, respectively. Additionally, the optimal policy for MED number of effects vs. MED capacity is developed and presented in Table 6.

Table 6. Optimal policy for MED number of effects versus MED capacities

Optimum number of effects	Min. capacity limit (kg/s)	Max. capacity limit (kg/s)
6	30	55
7	55	94
8	95	150
9	151	270

Scenario #1. The optimization formulation is solved without any constraint on the seawater mass flowrate or water recovery. The solution is shown by Figure 16. Three MED units are installed in interval 1, 10, and 15. In the period of sluggish demand increase (e.g. year 20-30), retrofit of the largest MED unit with two additional effects was included in the solution. This exploits the advantage of the retrofit option: modest increase in production with positive gain in thermal efficiency.

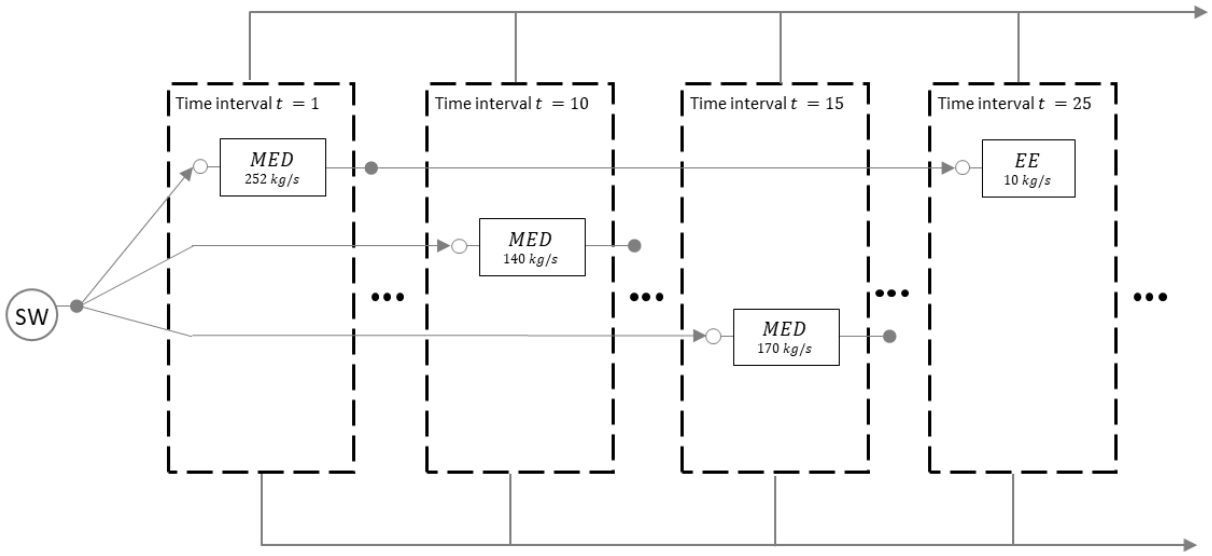

Figure 16. Results for scenario #1 (case study #2)

Scenario #2: MED units are limited in water recovery by the maximum salinity in brine. Hence, with the introduction of a constraint on seawater feed, MD became a constituent of the optimal flowsheet to satisfy the required water demand with the limited seawater feed through brine treatment. MD was introduced to the flowsheet at year 15 with Thea total area of MD is 10,800 m^2 producing a total of 54 kg/s. The total MD capital investment 9.87M. The solution is shown by Figure 17.

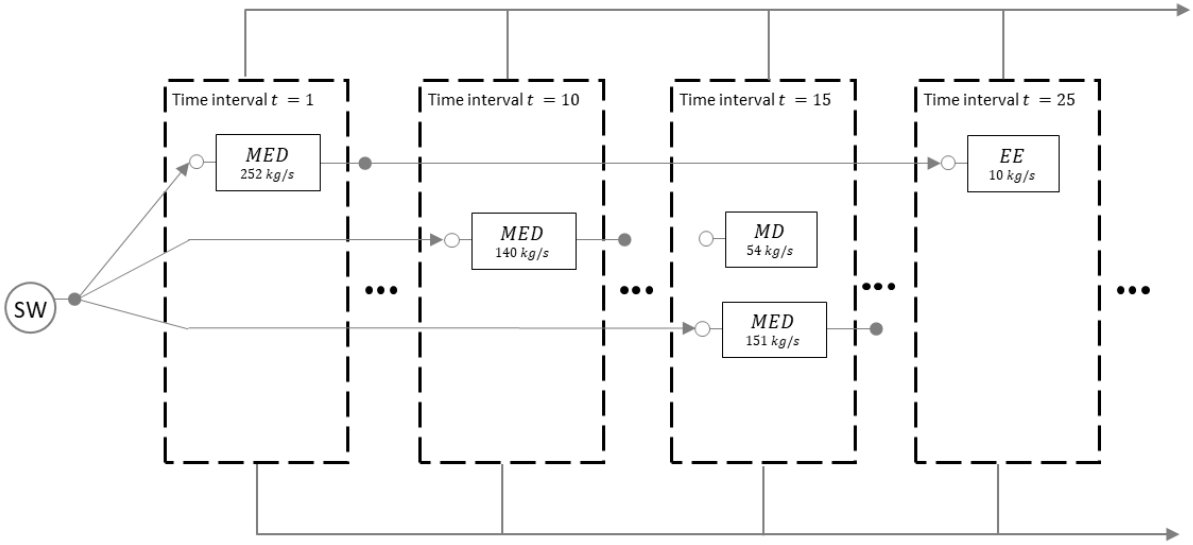

Figure 17. Results for scenario #2 (case study #2)

CHAPTER IV

OPTIMAL DESIGN AND SCHEDULING OF SOLAR-ASSISTED MD DOMESTIC DESALINATION SYSTEMS

4.1 Introduction

Despite the abundance of water in our plant, access to clean drinking water is one of the greatest global challenges facing humanity. The United Nation has ranked it second among global challenges following climate change (Glenn et al., 1997). In spite of the ambitious goals and achievements of the UN in this front, over 800 million people worldwide still lack access to drinkable water (Mapunda et al., 2018). One factor for this problem is the nonexistence of a centralized water network in many urban areas as governments struggle to cope with population growth and cities' expansion (Mapunda et al., 2018).

A feasible solution to the global water shortage problem is desalination. Desalination can be categorized into three major classes: thermal, membrane, and chemical technologies. Generally, desalination technologies are characterized by high-energy intensity, which represents a challenge for utilizing desalination in urban areas due to absence or limited conventional fuel distribution network.

Solar-assisted desalination is a potential fit for small urban potable water demand due to its decentralized nature and partial or full energy self-sufficiency. Sustainability is another advantage of solar-assisted desalination as its renewable energy source assuages the high-energy demand on conventional fossil fuel. Luckily, much of the water shortage problem exists in areas with abundance of solar power. For example, 43% of the world potable water shortage resides in the sub-Saharan region (Adams & Zulu, 2015). In recent years, the development of both

desalination technologies and solar power harvesting technologies have improved the competitiveness of solar-assisted desalination and attracted much research in this field. In desalination, for example, membrane technologies have made great strides in improving their durability and efficiency. Developments in metallurgies and coatings in water solar heaters, new concentrating technologies, and cheaper photovoltaic panels are few examples of key improvements in solar power harvesting. These developments alongside the developments in the membrane distillation technology are the motives for this research.

This research introduces a framework for the synthesis, optimization, and scheduling of small-scale solar-assisted membrane distillation desalination system. The work introduces the following contributions in this domain that are distinct from other literature by providing:

- Simultaneous design of the solar collectors and MD distillation system. The simultaneous optimization includes the sizing of the two systems, number and type of collectors, and operating variables such as targeted hot water temperature.
- Heat load optimization between conventional and solar energy. Load distribution of heating has implications on both fixed and operating costs of the two subsystems.
- Scheduling of solar-energy collection and preheated water dispatch. Optimization of the operational schedule of the system is influenced by the variability of solar power harvesting potential over time and tradeoffs evolving from first principles of heat and mass transfer in the system.

4.2 Literature Review

4.2.1 Solar Collectors

Solar power can be harvested either as thermal energy (i.e. thermal collectors or solar water heaters) or as electric power (i.e. photovoltaic panels). The advantage of solar thermal collection in desalination applications is the direct usage of solar radiative thermal energy without the conversion losses associated with electric solar system.

Solar water heaters (SWH) technologies can be classified into two major categories viz. concentrating solar power (CSP) and non-concentrating solar power. CSP, which deploys various technologies to concentrate solar irradiation for higher performance, is characterized by higher complexity and higher capital cost. Non-concentrating solar power covers an array of technologies that can be subcategorized into natural circulation (i.e. negative) or forced circulation (i.e. positive) systems (Sadhishkumar & Balusamy, 2014). The focus of this research is on the natural circulation SWH for two primary reasons. As indicated by Sadhishkumar and Balusamy (2014), the majority of the research on non-concentrating technologies is focused on forced circulation systems. This is likely driven by researchers striving to improve the modest performance of SWH systems. Yet, natural-circulation systems can be a good-enough solution in many applications due to their simplicity and lower capital and operating cost. Among the two major types of natural circulation SWHs: Integrated Collector Storage (ICS) and Flat Plate Thermosiphonic Unit (FPTU). Both systems are shown by Figure 18. The simplicity of the ICS systems gives a great advantage in the with a thermal desalination unit making the system compact and more economically attractive, two important features for small water demands.

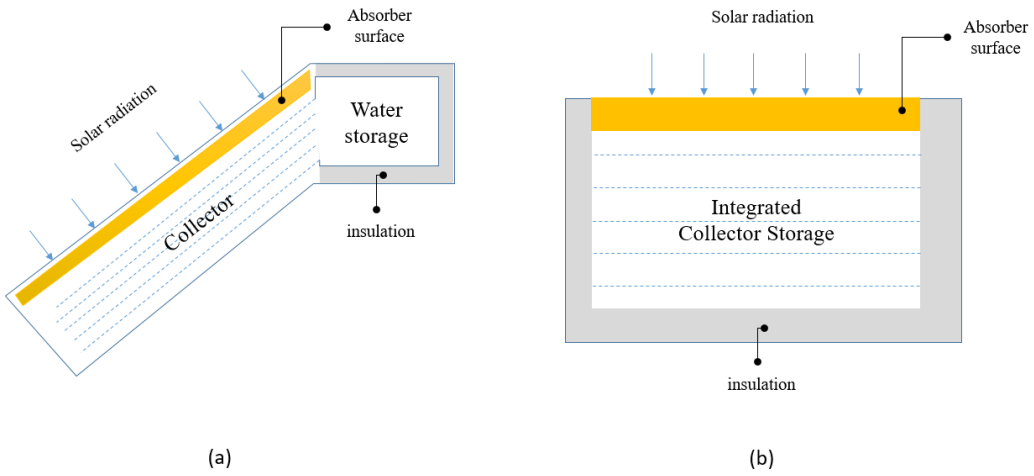

Figure 18. Schematic of thermal solar collectors (a) FPTU (b) ICS

ICS configuration introduces some disadvantages and design issues. High convective heat losses (i.e. at night and cold weather condition), intermittent operation of the solar heating system, and limited scalability are some of the challenges hosted by a hybrid desalination system with thermal solar collection, all considered in this research. For convenience, ICS is commonly referred to in this chapter as “solar-heating tank”.

4.2.2 Solar Water Desalination

A plethora of research to demonstrate the hybridization of solar power with different desalination technologies exists. Fiorenza, Sharma, and Braccio (2003) has carried a techno-economic evaluation of a solar-powered water desalination plant with a capacity between 500 to 5,000 $\frac{m^3}{day}$. A research summary on the integration of solar energy with various desalination technologies is listed in Table 7.

Table 7. Previous research on solar-driven/solar-assisted water desalination

Desalination technology	**Research**
Reverse osmosis (RO)	Mohamed, Papadakis, Mathioulakis, and Belessiotis (2008) Sajjad and Rasul (2015)
Multi-stage flash (MSF)	Hou (2008) Alsehli, Choi, and Aljuhan (2017)
Multi-effect distillation (MED)	Milow and Zarza (1997) Sharaf, Nafey, and García-Rodríguez (2011) Mabrouk et al. (2016)
Membrane distillation (MD)	F. Banat and Jwaied (2008) Hsuan Chang, Wang, Chen, Li, and Chang (2010) H Chang, Chang, Ho, Li, and Wang (2011) Saffarini, Summers, and Arafat (2012)
Electrodialysis (ED)	Ishimaru (1994) Ortiz et al. (2008) Fernandez-Gonzalez, Dominguez-Ramos, Ibañez, and Irabien (2015)

Fewer studies were conducted on the optimization of solar desalination plants. Sajjad and Rasul (2015) has developed a model for the simulation and optimization of PV-RO hybrid small-scale desalination system using ASPEN PLUS™. Hsuan Chang et al. (2010) has proposed a design approach for solar-driven MD desalination system with two thermal loops based on a pseudo-steady state approach. An economic assessment of solar-powered MD system by F. Banat and Jwaied (2008) showed a potable water cost of $15-18 per m^3 in large MD desalination system. Zamen, Amidpour, and Soufari (2009) presents a cost optimization of a solar humidification-dehumidification desalination unit.

Among thermal desalination technologies, membrane distillation (MD) evolves as a competitive technology for small-scale systems. Its compactness, modularity, and utilization of low-grade heat are some of the edge-cutting advantages for MD. Unlike reverse osmosis (RO) which is the standard pressure-driven membrane desalination technology for small and medium systems, MD is thermally driven, a clear advantage when hybridized with solar thermal collectors. Recent advancements in membrane design and manufacturing have led to high-performance membranes with extended lifecycle. For example, a flux of 120 $\frac{kg}{m^2 \cdot hr}$ for a saline feed of 3.5wt% at a 353K (Zuo, Bonyadi, & Chung, 2016). However, operating cost of MD systems can be significant. One solution proposed in literature is coupling MD desalination with industrial facilities or renewable energy sources (Bamufleh et al., 2017). Additionally, applying systematic methodologies to the desalination system synthesis can bring about important cost-effective designs by considering design decision variables as well as operational variables (i.e. operation's scheduling).

4.3 Problem Statement

The objective of this work is to develop an integrated thermal-electric system for solar-driven seawater desalination. The key concept is to collect solar heat through a set of seawater storage tanks. The preheated seawater is then further heated through an auxiliary heating system that uses compressed natural gas, which is burned to provide heat to a recirculating heating medium. The hot seawater is then fed to a membrane distillation system (MD) which produces permeate suitable for drinking and other human needs. A portion of the reject stream is recycled back to the MD system to reduce the heat losses and to provide a large enough heat content to drive the membrane distillation. A photovoltaic (PV) solar system is also used to produce electric

power that can be used in pumping seawater, the reject, and in other electric needs by the system. It consists of a PV panels that converts sunlight into DC electricity, a solar charge controller that regulates the voltage and current and prevents battery overcharge, inverter that converts DC output to an AC current, and a battery to store electric energy. A schematic superstructure representation of the proposed system is shown in Figure 19.

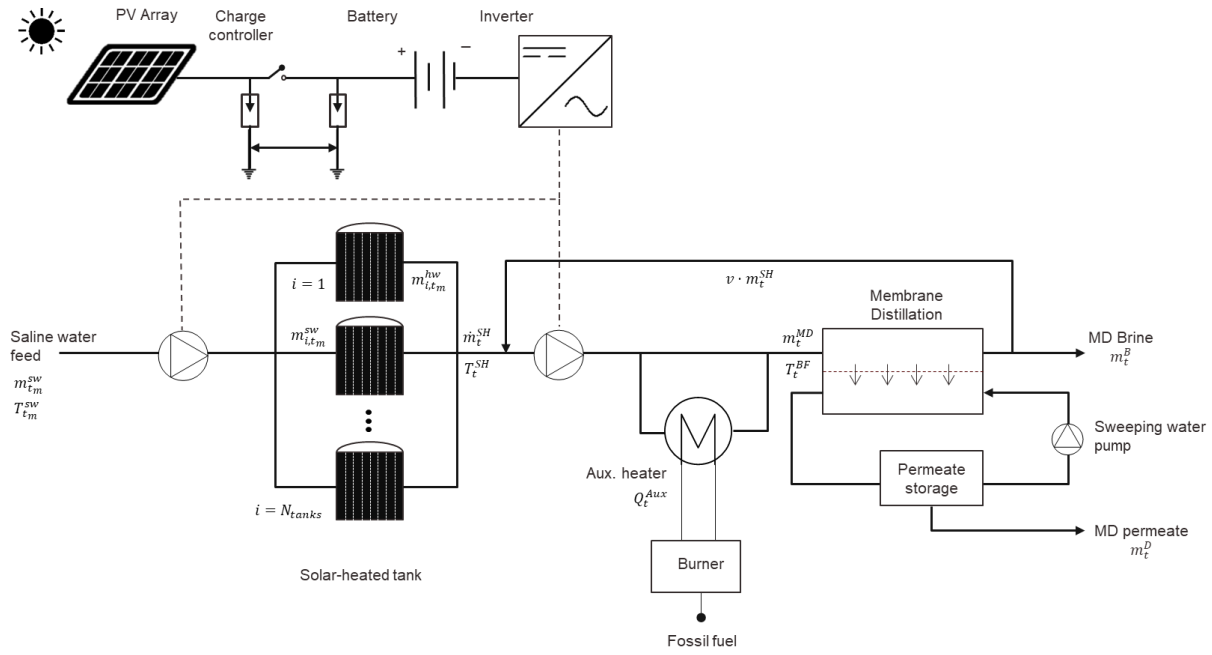

Figure 19. A superstructure representation of the solar-assisted MD desalination system

Thermal collection of solar energy in a tank is a simple approach to harvest the solar thermal energy by mounting a metal water tank to be heated by the sun. The performance of the system is governed by the efficacy of irradiation absorption and the system capacity to minimize heat losses. Heat loss (e.g. primarily convective but also includes radiative) is a major challenge to these systems. The problem statement may be stated as follows:

Given is a daily residential potable water demand, m_{day}^{D} in kg, at a given location, where solar irradiation data is readily available. The task is to synthesis on optimal design of the solar-assisted desalination system demonstrated in Figure 19 to satisfy the local demand. The heat required by the desalination process is provided by either a conventional heat source at a given unit price, c_{fossil}, or solar thermal heating or both. For solar thermal heating, a set of solar-heating tanks is used. The design of the tank such as its volume, shape, material of construction, etc. is fixed by initial screening and commercial availability. The optimization variables include:

- Number of the storage tanks
- Scheduling of solar-energy collection and preheated seawater dispatch
- temperature of the MD water feed
- the existence and heat duty of the auxiliary conventional heater
- MD design variables (i.e. membrane area, water recovery, brine recycle, etc.)
- Size of PV solar system

Next, the approach and formulation for the multi-period optimization problem is demonstrated.

4.4 Synthesis Approach

Due to the solar power inconsistency, the synthesis of the solar-assisted MD desalination is a multi-period optimization problem. Robust optimization of such problems is prohibitive due to its high non-convexity (i.e. nonlinear solar energy flux and MD mass flux). Our approach is to discretize the year into hourly intervals in which the daily hourly-average radiation data is available. At the end of each interval, the mass and enthalpy of each solar-heating tank is carried out to the subsequent interval. Our approach calls for tanks to assume one of four district operational stages. First, in the solar collection stage, the tank exclusively collect solar enthalpy

with no charging or discharging of water. In the hot water discharging stage, hot water from the tank is discharged for processing in the membrane distillation system. Saline water is fed to the tank in the charging stage. Lastly, the idle stage refers to the status of an empty tank in thermal equilibrium with the surrounding. The scheduling of all the tanks is assumed identical.

Two tasks are undertaken in this problem: synthesis and scheduling tasks. The scheduling task of the system involves finding the optimum sequence of stages for the tanks throughout the year, while the synthesis task deals with the optimal flowsheet synthesis. In section 4, we present a general formulation for the simultaneous optimization of the two tasks, followed by a discussion on solution techniques for the problem.

4.5 Optimization Formulation

First, the year is discretized into hourly counterparts, for which the hourly-average solar radiation data is available. The set $[T = t|t = 1,2, \dots ,24 \times 365]$ represents the hours in a day of a year. The subset $T_n \subseteq T$ represents the discretized hourly intervals for n^{th} day. The hourly solar irradiance is provided for each month and denoted, I_t. The number of potential solar-heating tanks comprises the set $[TANKS = i|i = 1,2, \dots , N_i]$. At any hourly interval (t), a solar heating tank takes one of four states, denoted by a set of binary variables: solar-heat collection, $BIN_{i,t}^{s}$, hot water discharging, $BIN_{i,t}^{c}$, seawater water charging, $BIN_{i,t}^{d}$, or idle state, $BIN_{i,t}^{l}$,. The frequency and duration of each state for a tank is subject to optimization. The objective is to synthesize the system flowsheet and schedule its operation to minimize the total annualized cost (TAC). It is comprised of the annualized fixed and operating costs, of the system:

$$minimize\ TAC = AFC + \sum_{t} OC_t \tag{79}$$

where AFC is the annualized fixed cost of the system, while OC_t is the total operating cost of the system at t^{th} hourly interval. The sum of the interval's operating costs yields the annual operating cost (AOC). The annualized fixed cost is expressed as the sum of the annualized fixed cost of each main equipment unit of the system, which can be calculated from their installed capital cost:

$$AFC = K_{MD}CC_{MD} + K_{PV}CC_{PV} + K_{Aux}CC_{Aux} + K_{Tanks}CC_{Tanks} + K_{Pump}CC_{Pump} \quad (80)$$

where CC is the installed capital cost, and K is the capital charge factor for annualizing the capital cost. This factor is equal to the inverse of the equipment's service life in the case of using the linear depreciation method and end-of-life zero book value. The installed capital cost for each equipment unit can be expressed in terms of its corresponding design parameters, which is usually expressed through a power law expression. MD capital investment, for example, may be correlated to the total membrane area. The costs of the solar PV equipment and auxiliary heater are expressed as a function of the total watt-peak rating and heat duty, respectively. For a subsystem or equipment, u, the general form for the capital investment estimator is given by:

$$CC_u = a_u \cdot DV_u^{scal} \quad (81)$$

where a is equipment-specific cost parameter, DV_u is the design or sizing parameter, and $scal$ is the power factor that capture the economies of scale of the cost function. Typical values for the power factor for process equipment is between 0.6-0.9. Table 8 illustrates our selection for the design variables for capital costing with the notation used in this formulation.

Table 8. Design variables for equipment installed costing

Installed capital cost	**Correlated with**	**Notation**
CC_{MD}	Number and area of MD modules	A_{MD}, N_{Design}^{MD}
CC_{Aux}	Auxiliary heater heat duty	Q_{Design}^{Aux}
CC_{Tanks}	Number and size of solar-heating tanks	N_{Tanks}, V_s
CC_{PV}	Total watt-peak rating & Battery capacity	P_{Design}^{PV}, $P_{battery}$
CC_{Pump}	Pumps Shaft power	P_s^{main}, $P_s^{cooling}$

The two primary operating cost are associated with MD and auxiliary heating. Other operating cost elements are either sustainably satisfied through solar thermal heat and electricity or neglected (i.e. PV maintenance).

$$OC_t = OC_t^{MD} + OC_t^{Aux} \tag{82}$$

where OC_t^{MD} and OC_t^{Aux} are the non-heating membrane operating cost and operating cost of auxiliary heating, respectively. The non-heating membrane cost is associated with the MD cooling cycle, MD recycling, and membrane maintenance. It is expressed typically as a function of key design variables, DV_{MD}, and operating variables, $OV_{MD,t}$, such as water recovery, recycle ratio, and feedwater mass flowrate. Due to the multiperiod nature of the problem, note that operating variables are expressed as a function of time:

$$OC_t^{MD} = f(DV_{MD}, OV_{MD,t}) \tag{83}$$

Auxiliary heating cost is directly calculated from the unit cost of the conventional fossil fuel as given by:

$$OC_t^{Aux} = c_{fossil} \cdot Q_t^{Aux} \tag{84}$$

where Q_t^{aux} is the heat supplied by auxiliary heater at t^{th} interval. The objective function (79) is subject to a set of constraints constituting the mass and heat balance of the system, the protocol mandated by the problem formulation, and boundary limits.

4.5.1 MD and Auxiliary Heater

The distillate water produced each day must meet or exceed the water demand as stipulated in the problem statement:

$$m_{day}^D \geq \sum_t m_t^D \quad \forall t \in T_n \tag{85}$$

where m_{day}^D is the fixed daily water demand in kg. m_t^D is the interval's distillate production, which is calculated from the water transmembrane flux, J_t^w, and total membrane area.

$$m_t^D = (A_{MD} \cdot N_t^{MD}) \int_t^{t+1} J_t^w \; dt \tag{86}$$

where A_{MD} is the modular-unit area of the membrane and N_t^{MD} is the number of module available at time interval. The transmembrane water flux is expressed as a function of the membrane permeability and the water vapor pressure difference across the membrane.

$$J_t^w = B_t^w \Delta p_t^w \tag{87}$$

where B_t^w is the membrane permeability and Δp_t^w is the water vapor pressure difference. Both parameters are highly dependent of the membrane feed temperature. Intuitively, the system flowsheet will assume the maximum number of membrane modules as given by:

$$N_{Design}^{MD} \geq N_t^{MD} \tag{88}$$

The transmembrane flux is correlated to membrane permeability and water vapor pressure difference across the membrane (Souhaimi & Matsuura, 2011). It is highly dependent on the operating temperature as both membrane permeability and water vapor pressure are temperature functions. The membrane feed temperature is denoted T_t^{BF} and is correlated to the auxiliary heat load:

$$Q_t^{Aux} = m_t^{MD} c_p \left(T_t^{BF} - T_t^{final}\right) \tag{89}$$

where m_t^{MD} is the membrane mass heated by auxiliary heating during the t^{th} interval. c_p is the specific heat capacity of saline water. T_t^{final} is the temperature of the solar-heated water at the discharging interval, calculated in the heat balance of the solar-heating tanks. Saline water heated in the solar heater tanks and mixed with the MD recycle flow is fed to the auxiliary heaters to boost the temperature of the MD feed to the optimal temperature. The task distribution between solar thermal heating and auxiliary heating is subject to optimization. The total mass fed to the auxiliary heater is expressed in terms of the hot water mass from the solar tanks:

$$m_t^{MD} = (1 + v) \cdot m_t^{hw} \tag{90}$$

where v is the ratio of the recycle mass to the hot water mass from the solar tanks. The membrane mass and component balance is given by:

$$m_t^{hw} = m_t^D + m_t^B \tag{91}$$

$$x_f \cdot m_t^{hw} = x_b \cdot m_t^D \tag{92}$$

where m_t^{hw} and m_t^B are, respectively, the water mass fed to MD and brine rejected from MD at the t^{th} in kg. x_f and x_b are the MD feed and brine salinity. For the sizing of the sweeping water tank and pump in the MD system, we estimates, first, the cooling load in the module:

$$Q_t^{cooling} = \frac{m_t^D \cdot H_{vw}}{\eta_{MD}} \tag{93}$$

where $Q_t^{cooling}$ is the cooling duty in MD in kJ. H_{vw} is the latent heat of vaporization, kJ/kg. η_{MD} is the thermal efficiency of MD. The cooling duty is provided through the sensible heat in the sweeping water. Assuming the permeate leaves MD at approximately the temperature of the feed (e.g. T_t^{BF}), the cooling duty may be expressed as follows:

$$\frac{m_t^D \cdot H_{vw}}{\eta_{MD}} = m_t^{cooling} \cdot c_p \, (T_t^{BF} - T^{BP}) \tag{94}$$

where $m_t^{cooling}$ is the sweeping water mass at a given interval in kg, and T^{BP} is the the bulk temperature at the MD permeate side. The tanks is sized to provide the required capacity to store all-day sweeping water mass for adequate heat dissipation:

$$\rho_w \cdot V_c \geq \sum_t m_t^{cooling} \quad \forall t \in T_n \tag{95}$$

where V_c is the sweeping water tank volume in m^3, and ρ_w is the density of the permeate water.

4.5.2 Solar-Heating Tanks

The constitutive equations for the solar thermal heating of saline water is presented next. The mass balance on the solar heating tanks involves buildup and depletion of water in the tanks due to the batch nature of the process. In its discretized form, the mass accumulation of water in the tanks is given by:

$$m_{i,t}^{final} = m_{i,t}^{initial} + m_{i,t}^{sw} - m_{i,t}^{hw} \quad \forall i \forall t \tag{96}$$

where $m_{i,t}^{initial}$ and $m_{i,t}^{final}$ are the initial and final water mass in the tank, $m_{i,t}^{sw}$ is the saline water mass fed to the tank in the discretized interval in kg and $m_{i,t}^{hw}$ is the hot water discharge mass, kg. The modeling of the above variables is dependent on the status of the tank. The followed protocol for our system is that tanks shall only assume one state at any interval. Hence, the summation of the four binary variables designating the status of the tank at any interval must equal one:

$$BIN_{i,t}^{s} + BIN_{i,t}^{c} + BIN_{i,t}^{d} + BIN_{i,t}^{l} = 1$$

where $BIN_{i,t}^{s}$ is for solar-heat collection, $BIN_{i,t}^{d}$ for hot water discharging, $BIN_{i,t}^{c}$ for seawater water charging, and $BIN_{i,t}^{l}$ for idle state (i.e. empty tank). The initial mass inventory in the tank is equated to the final mass inventory from the preceding interval as in (97). The mass accumulation in the tank shall not exceed the volume of the tank, V_s, as in (98).

$$m_{i,t}^{initial} = m_{i,t-1}^{final} \quad \forall i \forall t \tag{97}$$

$$m_{i,t}^{final} \leq \rho_{sw} V_s \quad \forall i \forall t \tag{98}$$

where ρ_{sw} is the density of saline water in kg/m^3. V_s is the volume of the tank in m^3. Charging of seawater and discharging of hot water are modeled by (99) and (100). The lower and upper limits are assigned based on the sizing limitation of the system's component (i.e. membrane minimum flow, pump minimum flow, etc.).

$$BIN_{i,t}^{c} \cdot LL^{sw} \leq m_{i,t}^{sw} \leq BIN_{i,t}^{c} \cdot UL^{sw} \tag{99}$$

$$BIN_{i,t}^{d} \cdot LL^{hw} \leq m_{i,t}^{hw} \leq BIN_{i,t}^{d} \cdot UL^{hw} \tag{100}$$

where LL^{sw} and UL^{sw} are the lower and upper limits for the saline water in an interval. LL^{hw} and UL^{hw} are the lower and upper limits of the hot-water mass in an interval as dictated by the MD manufacturer design. To model the condition of no mass in the tank during an idle state, the following constraint is introduced, where the $\rho_{sw}V_s$ constitutes the maximum mass in the tank:

$$\left(1 - BIN_{i,t}^{l}\right) \rho_{sw} V_s \geq m_{i,t}^{initial} \tag{101}$$

The mass balance on the saline water feed splits to the solar heating tanks is given by:

$$H_{i,t}^{final} - H_{i,t}^{initial} = H_{i,t}^{in} - H_{i,t}^{out} + H_{i,t}^{solar} - Q_{i,t}^{loss} \quad \forall i \forall t \tag{102}$$

where $H_{i,t}^{initial}$, and $H_{i,t}^{final}$ are the initial and final enthalpy of the tank in kJ. $H_{i,t}^{in}$and $H_{i,t}^{out}$ are the interval enthalpies associated with the charged and discharged masses, respectively, in kJ. $H_{i,t}^{solar}$ is the absorbed thermal energy from solar irradiance at a given interval in kJ, whereas Q_t^{loss} denotes the tank's heat losses (i.e. convective and radiative). The initial enthalpy of an interval is equated to the final enthalpy of the preceding interval:

$$H_{i,t}^{initial} = H_{i,t-1}^{final} \quad \forall i \forall t \tag{103}$$

Basic constitutive equation for the enthalpy of inlet saline water is expressed by:

$$H_{i,t}^{in} = m_{i,t}^{sw} \cdot c_p \cdot T^{sw} \tag{104}$$

$$H_{i,t}^{out} = m_{i,t}^{sw} \cdot c_p \cdot T_{i,t}^{final} \tag{105}$$

$$H_{i,t}^{final} = m_{i,t}^{final} \cdot c_p \cdot T_{i,t}^{final} \tag{106}$$

where T^{sw} is the saline temperature in K. $m_{i,t}^{sw}$ is the water fed to the i^{th} tank in kg. $T_{i,t}^{final}$ is the final temperature in the tank in K. The model proposed by (Bakir, 2006) is adopted to correlate the solar enthalpy with an absorbance-transmittance coefficient, α_s. The coefficient is dependent in the design parameters of the tank such as shape and material of construction as well as location factors:

$$H_{i,t}^{solar} = \alpha_s \, A_s \, I_t \tag{107}$$

where A_s is the surface area of the tank in m^2. I_t is the available solar irradiance in the t^{th} interval in kJ/m^2. In this formulation, it is assumed that no solar collection occurs when the tank is in the state of discharging, charging, or idle:

$$\left(1 - BIN_{i,t}^{s}\right) \cdot LL^{solar} \leq H_{i,t}^{solar} \leq \left(1 - BIN_{i,t}^{s}\right) \cdot UL^{solar} \tag{108}$$

where LL^{solar} and UL^{solar} are lower and upper limits for the hourly solar enthalpy. Heat losses are expressed as a function of the tank's design variables, DV_s, tank's operating variables, $OV_{i,t}$, the air temperature, T_t^{air}:

$$Q_{i,t}^{loss} = f_{loss}(DV_s, OV_{i,t}, T_t^{air}) \tag{109}$$

The mass balance of the mixing of the tank's hot water at any interval are given by (110), where m_t^{hw} is the hot water mass in kg.

$$m_t^{hw} = \sum_i m_{i,t}^{hw} \tag{110}$$

4.5.3 Pumping and Solar Photovoltaic (PV)

The system consists of two pumps, driven by electric motors: the feed pump used for the charging and discharging of water from the tank, and the MD sweeping water pump. The electricity is supplied by the solar PV system. The shaft power of each pump is expressed as a function of its volumetric flow rate and pressure head with an assumed efficiency. The general form of the function is given by:

$$P_s = (m) \cdot \frac{\Delta p}{\rho \cdot \eta_{pump}} \tag{111}$$

where P_s is the shaft power of the pump, Δp is the pressure head, m is the mass flowrate, and η_{pump} is the pump's efficiency. Assuming a constant pressure head and efficiency, the shaft power is designed based on the maximum volumetric flowrate assumed from the mass balance over time (i.e. maximum $m_t^{cooling}$ for sweeping water pump). The total Watt-hours per day of the pumps is calculated from the shaft powers and adjusted for system's energy loss and panel's generation factor to estimate the total Watt-peak rating (P_{peak}^{PV}). Given the unit size for a PV module (P_{unit}^{PV}), an integer number of required PV modules (N_{PV}) is provided by:

$$N_{PV} \cdot P_{unit}^{PV} \geq P_{peak}^{PV} \tag{112}$$

The battery capacity, $P_{battery}$, is designed to store sufficient energy to operate the pumps after sunset. The design of the battery accounts for the following factors: battery loss, depth of discharge, nominal battery voltage, and back up. The PV system cost may be expressed as a function of the PV panel and battery sizing. The total installed capital cost of pumps is correlated to the shaft power as in:

$$f_{pv}\left(CC_{PV}, N_{PV}, P_{peak}^{PV}, P_{battery}\right) = 0 \tag{113}$$

$$CC_{pump} = (P_s) \tag{114}$$

where f_{pv} and f_p are vectors of costing equations of PV system and pumping system, respectively.

The above formulation yields an MINLP optimization that needs to be solved simultaneously for the generation of the optimal solution. Figure 20 illustrates our solution technique of the optimization problem. It starts with the realization of the inadequacy of the solar-heating tank to achieve a high-enough temperature for an appreciable MD flux without auxiliary heating. For example, previous research on the finite element analysis of spherical solar-heating tanks shows a maximum hot water temperature of 35-45C (Bakir, 2006; Gáspár, BALAN, Jäntschi, & ROS, 2012; Samanta & Al Balushi, 1998). The lower efficiency (i.e. lower hot-water temperature) necessitates auxiliary heating for an appreciable flux in the MD system. With auxiliary heating, MD feed temperature is fixed across the design period but subject to optimization.

The sequential steps of the proposed solution technique in Figure 20 are as follows:

- A pre-synthesis optimization of the water recovery of the system is carried out. Based on a pre-synthesis cost analysis of the system equipment, distillate requirements, and the overall process constraint, water recovery is pre-optimized. For example, in systems where MD cost is grossly dominating the overall system cost function, local water recovery optimal with respect to the MD system is determined part of the global optimal policy. For cases where MD system cost is not dominant, the optimal recovery ratio can be determined through a brute-force search method. Having fixed the recovery ratio, water mass feed to

both subsystems: solar collection and MD distillation is determined through the constitutive mass balance equations.

- With the mass load determined for the system's saline feed, the number of solar-heating tanks is determined based on the design variables of the individual available commercial tanks. The system is decomposed into two main subsystem: solar heating and MD.
- Through discretization, the multi-period net solar enthalpy is used to optimize the scheduling of the operation of the solar tanks for the maximization of solar collection, and hence, the minimization of auxiliary heating. This approach in determining the global optimization for the subsystem is based on Bellman's principle of optimality (Bellman, 1954). It states that "an optimal policy has the property that, whatever the initial state and the initial decision are, the remaining decisions must constitute an optimal policy with regard to the state resulting from the first decision." Similarly, the design variables of the MD subsystem such as the feed temperature and recycle ratio are optimized locally.
- The auxiliary heating system is designed along with the power system. The overall objective function from all subsystems are calculated to identify the cost results and the optimal solution.

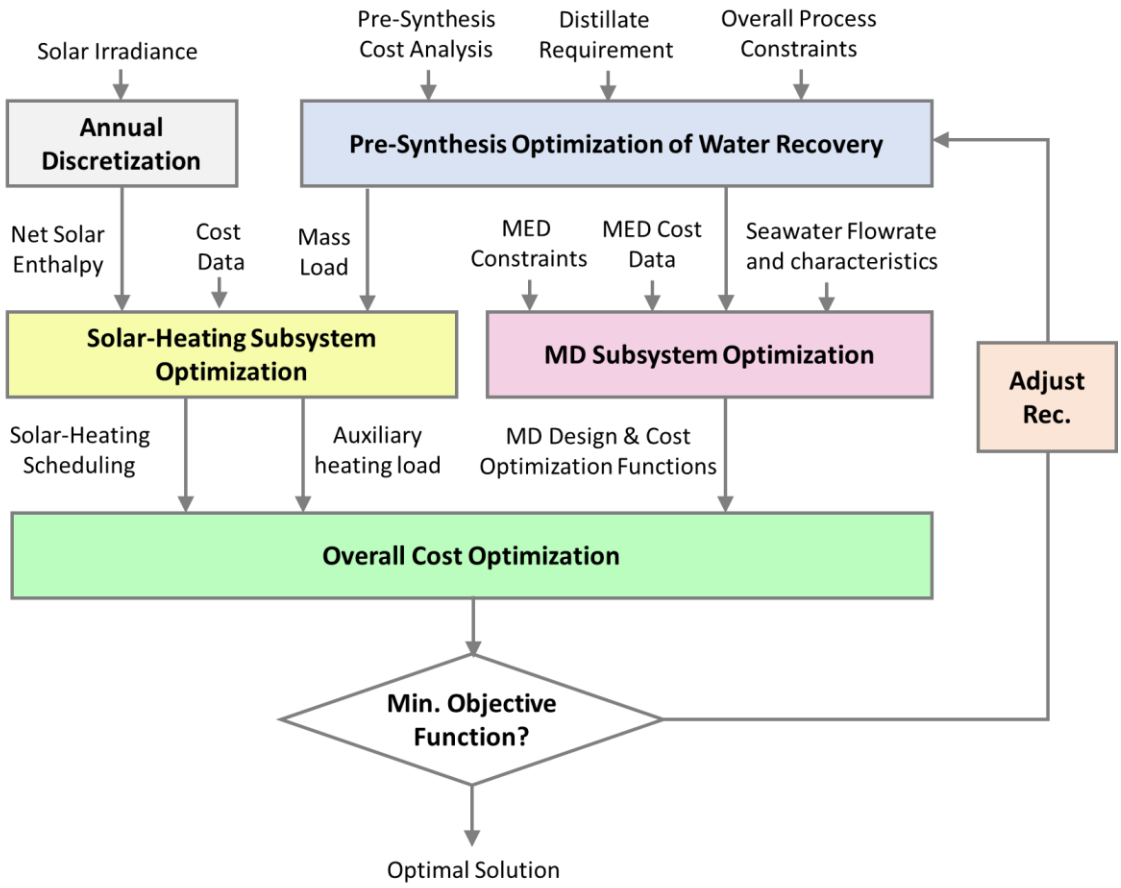

Figure 20. Solution approach flowchart for the solar-assisted MD desalination synthesis

4.6 Case Study

4.6.1 Case Study Description

A solar-assisted desalination system is to be designed for the city of Jeddah, Saudi Arabia. The system aims at sufficing the potable water need for a household of 5 persons. The World Health Organization (WHO) estimates water consumption per person between 50-100 liters (0.05-0.1 m^3) to ensure most basic needs. Therefore, the total design capacity for the envisaged system is 0.5m^3 of desalinated water. The feed is seawater with a salinity of 35‰. The average monthly temperature of seawater is given by Table 9.

Table 9. Average seawater temperature for Jeddah city

Month	Temperature (K)
January	298.6
February	299.0
March	299.4
April	300.1
May	301.3
June	302.0
July	304.4
August	304.6
September	304.1
October	302.8
November	301.8
December	301.4

Note: Data for seawater temperature in Jeddah, Saudi Arabia from Watertemperature.org (2015)

Stainless steel water storage and thermal collection tanks are to be used as a source of solar renewable energy for heating with a transmittance-absorbance factor of 50%. The unit cost of 0.4 m^3 stainless-steel cylindrical tanks (0.5-m diameter, 2-m height) is $1,000. A gas-fired heater (at a cost of $3.0 GJ) may be used to supplement the solar energy collected by the tanks. For estimating the solar intensity, the half sine model is used:

$$I_t = I_{noon} * sin\left[\frac{180 * (t - t_{sunrise})}{t_{sunset} - t_{sunrise}}\right] \quad (115)$$

where I_t is the solar intensity, at time t. $t_{sunrise}$ and t_{sunset} correspond to the times of sunrise, sunset on the considered day. I_{noon} is the peak solar irradiance level at solar noon on the considered

day. For the city of Jeddah, Abdelhady, Bamufleh, El-Halwagi, and Ponce-Ortega (2015) reported the following correlation:

$$I_{noon} = -0.009\, N_{day}^2 + 3.1812\, N_{day} + 643.7 \quad (116)$$

where N_{day} is the day number and I_{noon} is in W/m^2. Combining (37 and (38), we obtain:

$$I_t = (-0.009 N_{day}^2 + 3.1812\, N_{day} + 643.7) * \sin\left[\frac{180 * (t - t_{sunrise})}{t_{sunset} - t_{sunrise}}\right] \quad (117)$$

For MD, a polypropylene hollow-fiber membrane MD020CP2N (manufactured by Microdyn) is used. The hollow fibers have a length of 0.45 m, an inside diameter of 1.5 mm, and an outside diameter of 2.8 mm. Details of these modules are given by Al-Obaidani et al (Al-Obaidani et al., 2008). The maximum operating temperature of the membrane is set at 350K and maximum water recovery at 80%. The minimum mass flowrate to the membrane module is 1.5 kg/s. The modeling of these modules given by Elsayed et al. (Nesreen A. Elsayed, Barrufet, & El-Halwagi, 2014) includes the following main equations. The membrane permeability, B_w, is expressed as a function of the average membrane temperature, T_m:

$$B_w = B_{wb} \cdot T_m^{1.334} \quad (118)$$

where B_{wb} is the temperature-independent base value of permeability (for this module: $B_{WB} = 7.5 \cdot 10^{-11} \frac{kg}{m^2 \cdot s \cdot Pa \cdot K^{1.334}}$). The thermal efficiency for vaporization in the MD module, η_{MD}, is adopted from (Lokare, Tavakkoli, Khanna, & Vidic, 2018) expressed as a function of water recovery. The membrane unit cost is \$90/m^2 and a Lang factor of 5 is used for the estimation of the total installed cost. The annualized fixed cost of the MD network, AFC_{MD}, is given by:

$$AFC_{MD} = 58.5 \cdot A_{MD} + 1{,}115 \cdot m_{MD} \quad (119)$$

where A_{MD} is the area of the membrane in m^2 and m_{MD} is the flowrate of the saline water entering the MD in kg/s. The non-heating operating cost data for MD shown in Table 10.

Table 10. Non-heating operating cost of MD

Cost item	**Value**	**Unit**	**Reference**
Pretreatment & Labor	0.0490	$/tonne of raw feed	Kesieme et al. (2013)
Brine Disposal	0.0015	$/tonne of brine	Al-Obaidani et al. (2008)

A set of PV panels, each at 110W capacity, supplies both the feed and sweeping water pumps with the required electrical power. The build-of-system (BOS) cost of the PV system is $3.25/W. The objective of the optimization formulation is to minimize the total annualized cost, TAC as in (79).

4.6.2 Solution

Following the proposed approach, the pre-synthesis optimization of water recovery is carried out. Higher water recovery yields many economic advantages including lower brine disposal, lower temperature polarization due to higher flowrate in the membrane, and higher thermal efficiency. But, it also results in higher feed salinity (i.e. lower water vapor pressure), which can cause membrane area to increase. Other disadvantages of higher recovery includes higher power cost due to high recirculation and higher pretreatment cost. Figure 21 shows the results of the water recovery pre-optimization. The annual operating and fixed cost, as well as the

total annualized cost, per cubic meter of distilled water are plotted. The optimum water recovery is 65%.

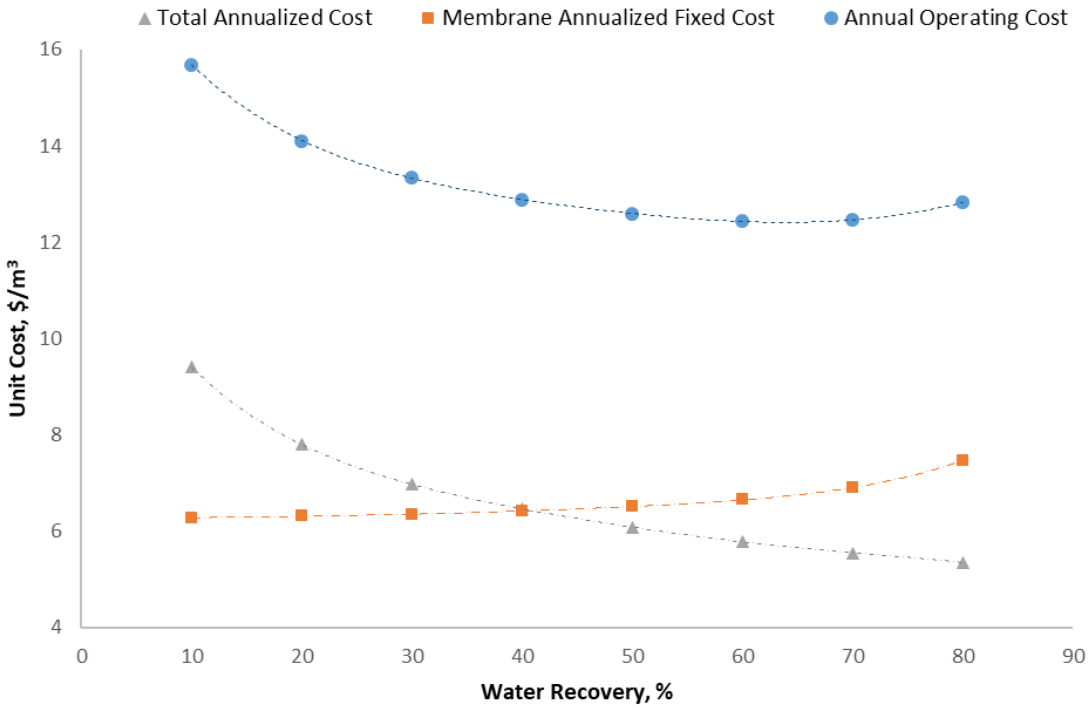

Figure 21. Water recovery optimization (case study #3)

At the optimum recovery, the required daily saline water is $0.77m^3$. Therefore, two commercial tanks specified in the problem statement are adequate to provide the required saline water with a one-cycle per day scheduling (i.e. discharge once a day). One tank coupled with two-cycle schedule is another viable alternative. Next, the solar radiation data is discretized as a precursor to the optimization of the scheduling of the solar collection. The convectional losses from the tank is estimated by:

$$Q_t^{loss} = \alpha_{cv} \cdot A_s \left(T_t^{final} - T_t^{air}\right) \tag{120}$$

where α_{cv} is the convection coefficient in W/(m^2 K) and assigned an average value of 20 for free convectional losses in stainless steel water tank. A_s is the tank's surface area in m^2. T_t^{air} is the air temperature in K. The hourly air temperature for Jeddah city is taken from Meteonorm's database. With higher number of cycles (i.e. multiple charging/discharging in a day), the temperature in the tank is not allowed to reach high temperature and therefore minimizing convectional losses. However, this comes at the cost of losses in solar collection as the tank during charging/discharging assumes no solar collection. As shown in Figure 22, a schedule of two cycles yields the highest enthalpy at 1800 Wh/m^2. Additionally, it results in lower capital expenditure for solar-heating tanks with only one tank compared to 2 heating tanks with a one-cycle scheduling.

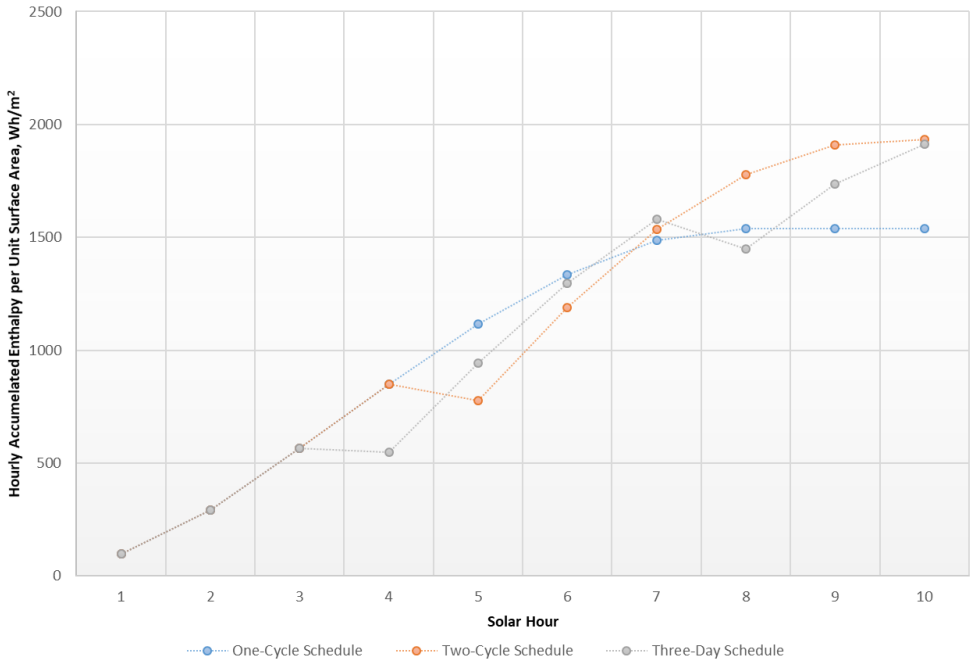

Figure 22. Solar heating scheduling optimization (case study #3)

The results of the optimization of MD as well as the sizing of the remaining equipment is listed in Table 11. The optimal flowsheet consists of one solar-collecting tank scheduled to discharge twice a day and an MD desalination system with 16.8 m^2 of membrane area. With a module area ranging from 50-200m^2, one MD-module is adequate for the system. An estimated 9 PV panels are required for the system. For 12-V battery with depth and loss factors of 0.6 and 0.85, respectively, the design Amps-hours for the battery is 407 Ah. The total annualized cost for the system based on a service life of 4 years for the membrane and 10 years for the remaining equipment is $4,150.

Table 11. Results of solar-assisted MD desalination case study

Description	Result	Unit
Number of Tanks	1	
Number of discharge cycles	2	
MD membrane area	16.8	m^2
Number of MD modules	1	
MD feed temperature	350	K
Recycle ratio	4.69	
Water recovery	65%	
Brine salinity	8.9%	
PV peak-hour rating	913	Wh
Number of PV panels	9	
Battery capacity	407	Ah
Auxiliary heater efficiency	90	%
Auxiliary heater size	220	kW
Fixed annualized cost	2,400	$
Annual operating cost	1,750	$
Total annualized cost	4150	$
Water unit cost	22.8	$/$m^3$

4.7 Experimental Validation

In collaboration with King Abdulaziz University in Saudi Arabia, a pilot solar desalination system is under development to complement and validate the analytical study. Phase I of the project will focus on optimizing the ICS heater in isolation of the downstream unit (i.e. MD). In phase two, more key elements of the design that are instrumental to the integration of the ICS with MD will be introduced. For example, the size of the conventional backup heating system will be considered. Additionally, the scheduling of the system as well as operability of the system will be

tested. For example, scale buildup, an anticipated challenge to the system operability will be addressed in the experimental work.

The prototype of the thermal solar collector has been constructed at King Abdulaziz University campus on December, 2017. Figure 23 shows pictures of the solar collector and the mounting skid.

Figure 23. Photos of the manufactured solar heater for the pilot testing

CHAPTER V

CONCLUSION AND RECOMMENDATIONS

5.1 Conclusion

Integral approaches to the synthesis of water desalination involving water energy nexus has been examined through the development of the modeling and design framework of three desalination design synthesis problems.

First, a research is presented on the optimization formulation of the synthesis of an integrated MED-MD desalination system with thermal coupling to industrial facility. The proposed approach started with determining the quantity and quality of the industrial excess heat. The optimization of design and operating variables of the hybrid MED-MD system is carried out through a discretization decomposition technique. A four-scenario case study is presented showing the impact of various design parameters and constraints on the optimum desalination system design.

In Chapter III, a multi-period optimization approach for the capacity-expansion planning of water desalination systems is introduced to satisfy a forecasted demand growth over a given time horizon. The approach was illustrated in a general formulation and on a special case for capacity expansion in MED desalination systems, where three options were considered for capacity expansion: grassroots MED, existing MED retrofits, and MD desalination. The presented formulation simultaneously optimizes design capacities, period of installation, as well as technology-specific design variables such as the number of MED effect, TBT, and MD feed temperature. A case study has been solved for three different scenarios to illustrate the merits of the presented approach. The results have illustrated the impact of considering alternative options

for capacity expansion on the optimal design. Notwithstanding the economic challenges facing emerging technologies, alternative options to meeting demand growth such as MD provide advantages to the system by providing valuable flexibility and modularity in the design stage to maximize economic return.

A design and scheduling approach for a skid-mounted solar-assisted membrane distillation (MD) system has been presented in Chapter IV. The developed framework simultaneously optimizes the solar collection and MD subsystem for the minimizing of total annual cost. The approach was illustrated in a case study where potable water was produced in a solar-assisted MD system at a unit cost of $\$22/m^3$. This work highlights the two primary economic opportunities for cost reduction in such desalination system. First, the MD membrane cost constitutes the dominant cost element in the system. Future improvements in the performance of the membrane or the mass commercialization of the technology would reduce the cost of the membrane making the illustrated desalination system more economically attractive. Economic viability might also be achieved through improvements in the thermal efficiency of solar-heating tank.

5.2 Recommendations for Future Work

The integral approaches developed in this research may be expanded through the following future work:

- Introduction of time-based performance models of desalination technologies. Many desalination plants such as RO and MD experience a deteriorating performance over their service life, which can have significant impact on the optimal synthesis of water systems.

- Inclusion of the sustainability return on investment metric to extend the results of this research to include the assessment of sustainability issues.
- Synthesis of the heat exchanger network for industrial facilities, integrated with MED-MD desalination system.
- Development of the capacity planning framework for water systems in eco-industrial parks (EIP). The work on water capacity planning in this research may be extended to EIP water system where both the chemical and water system are synthesized simultaneously.
- Completion of the experimental validation of the solar-assisted MD desalination in collaboration with King Abdulaziz University.

NOMENCLATURE

Chapter II Nomenclature

$A_{MED,n}$	MED evaporative evaporator area, m^2
B_n	Brine mass flowrate from n^{th} evaporator
c_{loss}	environmental losses factors for MD
D_n	distillate mass flowrate from n^{th} evaporator
F	seawater mass flowrate to MED
$h_{B,n}$	liquid enthalpy of the brine in n^{th} evaporator
$H_{D,n}$	vapor enthalpy in n^{th} evaporator
J_w	transmembrane water flux
k_m	thermal conductivity of membrane
K_w	overall permeability factor
K_w^K	Knudsen permeability factor
K_w^{mol}	molecular diffusion permeability factor
$\Delta H_{vw,s}$	heat of evaporation of external steam
M_w	molecular weight of water
Δp_w	water partial pressure difference across MD
$Q_{MED,n}$	heat load of n^{th} evaporator in MED
r	pore size of membrane in MD
$U_{MED,n}$	overall heat transfer coefficient in n^{th} effect
W_B^{MED}	brine mass flowrate from MED
W_{reject}^{MED}	Reject mass flowrate from MED to environment

W_f^{MD} MD feed mass flowrate

γ_w activity coefficient

τ membrane pore tortuosity

δ membrane thickness

θ temperature polarization coefficient

$\eta_{thermal}$

Chapter III Nomenclature

A_{HTFFE} area of MED evaporators, m^2

A_m area of MD module, m^2

AOC_t annual operating cost at t^{th} interval

$B_{i,t}$ brine flowrate of a subsystem, kg/s

B^t system's brine flowrate, kg/s

BV_t End-of-horizon book value of investments at t^{th} interval

c_{HU} unit price of heating utility

D_t system total distillate capacity at an interval, kg/s

$D_{i,t}$ subsystem's water capacity, kg/s

d_t water demand at an interval, kg/s

ΔD_t added distillate capacity at an interval, kg/s

$DV_{i,t}$ design variables of a subsystem

$F_{m_{i,t}}^{total}$ mass flowrate to the m^{th} inlet node, kg/s

$F_{n_{i,t}}^{total}$ mass flowrate for the n^{th} outlet node, kg/s

$F_{n_{i,t}}^{m_{i,t}}$	mass flowrate from n^{th} outlet node to m^{th} inlet node, kg/s
F^{sw}	seawater mass flowrate, kg/s
GOR	gained output ratio
H_{vw}	water heat of vaporization
$I_{i,t}$	binary variables for the existence of i^{th} configuration at t^{th} interval
J_w	water mass flux in MD, kg/(s.m^2)
M^s	MED steam mass flowrate, kg/s
NPV	net present value
N_{eff}	number of evaporative effects
$OV_{i,t}$	operating variables of a subsystem
Q_{evp}	heat duty of MED evaporative effect, W
REV_t	revenue at t^{th} interval
r	minimum rate of return
$SV_{i,t}$	state variables of a subsystem
SL	average subsystem service life
TCI_t	total capital cost of t^{th} interval
T_s	temperature of heating steam in MED, K
T_c	temperature of cooling medium in MED, K
U_{HTFFE}	overall heat transfer coefficient of evaporators, W/(m^2.K)
$x_{i,t}^d$	distillate salinity from a subsystem
$x_{i,t}^b$	brine salinity from a subsystem
x_t^d	overall distillate salinity of the system

x_t^b	overall brine salinity of the system
η	thermal efficiency
α	MED temperature-dependent design parameter
γ	ratio of MD recycle flowrate to feed
ξ	MD water recovery
λ_n	heat of evaporation at a given MED effect, W

Chapter IV Nomenclature

A_{MD}	single-module membrane area, m2
A_s	solar-heating tank surface area
a_u	capital cost parameter for equipment/subsystem
α_s	transmittance-absorbance factor of the heating tank
K	capital charge factor for annualizing capital cost
c_{fossil}	unit cost of fossil fuel, $\frac{\$}{kWh}$
c_p	specific heat capacity
m_{day}^D	daily demand of distilled water, kg
$scal$	power factor for capital costing
V_s	solar-heating tank volume, m^3
v	MD recycle ratio
x_f	saline water salt mass concentration
x_b	brine salt mass concentration
ρ_{sw}	density of saline water
ρ_w	density of distilled water

T^{sw}	saline water temperature
AFC	annualized fixed cost
B_t^w	membrane permeability
$BIN_{i,t}^c$	binary variable for a tank charging at t^{th} interval
$BIN_{i,t}^d$	binary variable for a tank solar collection at t^{th} interval
$BIN_{i,t}^d$	binary variable for a tank discharging at t^{th} interval
$BIN_{i,t}^l$	binary variable for a tank idle state at t^{th} interval
CC	total installed cost
DV	vector of design variables
H_{vw}	heat of evaporation
$H_{i,t}^{solar}$	tank's absorbed solar enthalpy
$H_{i,t}^{out}$	enthalpy of the discharged water from tank
$H_{i,t}^{in}$	enthalpy of the charged water from tank
$H_{i,t}^{initial}$	tank's initial enthalpy at t^{th} interval
$H_{i,t}^{final}$	tank's final enthalpy at t^{th} interval
I_t	solar radiation at time t
J_t^w	transmembrane water flux, $kg/(m^2 \cdot s)$
m_t^D	interval's distillate production, kg
m_t^{hw}	hot water temperature from solar heating system
m_t^{MD}	MD total water at t^{th} interval, kg
m_t^B	MD brine water at t^{th} interval, kg
$m_t^{cooling}$	D sweeping water at t^{th} interval, kg

$m_{i,t}^{initial}$ tank initial water inventory at t^{th} interval, kg

$m_{i,t}^{final}$ tank final water inventory at t^{th} interval, kg

$m_{i,t}^{sw}$ tank saline water at t^{th} interval, kg

$m_{i,t}^{hw}$ tank hot water discharge at t^{th} interval, kg

N_{PV} number of PV panels

N_t^{MD} variable number of membrane modules at t^{th} interval

N_{Design}^{MD} number of membrane modules

η_{MD} thermal efficiency of MD

OC_t operating cost for the t^{th} interval

$OV_{i,t}$ operating variables of i^{th} tank at t^{th} interval

P_{Design}^{PV} PV total watt-peak rating

P_s^{main} shaft power for the main feed pump

P_s^{main} shaft power of sweeping water pump

$P_{battery}$ total Ampere-hours of the battery

Δp_t^w water vapor pressure difference

Q_{Design}^{Aux} auxiliary design heat duty, kWh

Q_t^{Aux} auxiliary heat duty at t^{th} interval, kWh

$Q_t^{cooling}$ cooling duty in MD in kJ

TAC total annualized cost

T_t^{final} solar-heated water temperature at interval end

T_t^{BF} MD feed temperature

T^{BP} MD permeate temperature

V_c sweeping water tank volume

REFERENCES

Abdelhady, F., Bamufleh, H., El-Halwagi, M. M., & Ponce-Ortega, J. M. (2015). Optimal design and integration of solar thermal collection, storage, and dispatch with process cogeneration systems. *Chemical Engineering Science, 136*, 158-167.

Adams, E. A., & Zulu, L. C. (2015). Participants or customers in water governance? Community-public partnerships for peri-urban water supply. *Geoforum, 65*, 112-124.

Al-Aboosi, F. Y., & El-Halwagi, M. M. (2018). An Integrated Approach to Water-Energy Nexus in Shale-Gas Production, *Processes, 6*(5), 52.

Al-Obaidani, S., Curcio, E., Macedonio, F., Di Profio, G., Al-Hinai, H., & Drioli, E. (2008). Potential of membrane distillation in seawater desalination: thermal efficiency, sensitivity study and cost estimation. *Journal of membrane science, 323*(1), 85-98.

Al-Shammiri, M., & Safar, M. (1999). Multi-effect distillation plants: state of the art. *Desalination, 126*(1-3), 45-59.

Alasfour, F., Darwish, M., & Amer, A. B. (2005). Thermal analysis of ME—TVC+ MEE desalination systems. *Desalination, 174*(1), 39-61.

Alkhudhiri, A., Darwish, N., & Hilal, N. (2012). Membrane distillation: a comprehensive review. *Desalination, 287*, 2-18.

Alklaibi, A., & Lior, N. (2005). Transport analysis of air-gap membrane distillation. *Journal of membrane science, 255*(1), 239-253.

Alsaadi, A. S., Francis, L., Amy, G. L., & Ghaffour, N. (2014). Experimental and theoretical analyses of temperature polarization effect in vacuum membrane distillation. *Journal of membrane science, 471*, 138-148.

Alsaadi, A. S., Ghaffour, N., Li, J.-D., Gray, S., Francis, L., Maab, H., & Amy, G. L. (2013). Modeling of air-gap membrane distillation process: a theoretical and experimental study. *Journal of membrane science, 445*, 53-65.

Alsehli, M., Choi, J.-K., & Aljuhan, M. (2017). A novel design for a solar powered multistage flash desalination. *Solar Energy, 153*, 348-359.

Bakir, O. (2006). Experimental Investigation of a Spherical Solar Collector (Doctoral disseration, Middle East Technical University).

Bamaga, O., Yokochi, A., Zabara, B., & Babaqi, A. (2011). Hybrid FO/RO desalination system: Preliminary assessment of osmotic energy recovery and designs of new FO membrane module configurations. *Desalination, 268*(1-3), 163-169.

Bamufleh, H., Abdelhady, F., Baaqeel, H. M., & El-Halwagi, M. M. (2017). Optimization of multi-effect distillation with brine treatment via membrane distillation and process heat integration. *Desalination, 408*, 110-118.

Banat, F., & Jwaied, N. (2008). Economic evaluation of desalination by small-scale autonomous solar-powered membrane distillation units. *Desalination, 220*(1-3), 566-573.

Banat, F. A., & Simandl, J. (1998). Desalination by membrane distillation: a parametric study. *Sep. Sci. Technol, 33*(2), 201-226.

Bellman, R. (1954). The theory of dynamic programming. *Bulletin of the American Mathematical Society, 60*(6), 503-515.

Billinton, R., & Karki, R. (2001). Capacity expansion of small isolated power systems using PV and wind energy. *IEEE Transactions on Power Systems, 16*(4), 892-897.

Budhiraja, P., & Fares, A. A. (2008). Studies of scale formation and optimization of antiscalant dosing in multi-effect thermal desalination units. *Desalination, 220*(1-3), 313-325.

Chang, H., Chang, C., Ho, C., Li, C., & Wang, P. (2011). Experimental and simulation study of an air gap membrane distillation module with solar absorption function for desalination. *Desalination and Water Treatment, 25*(1-3), 251-258.

Chang, H., Wang, G., Chen, Y., Li, C., & Chang, C. (2010). Modeling and optimization of a solar driven membrane distillation desalination system. *Renewable Energy, 35*(12), 2714-2722.

Chernyshov, M. N., Meindersma, G. W., & de Haan, A. B. (2003). Modelling temperature and salt concentration distribution in membrane distillation feed channel. *Desalination, 157*(1), 315-324.

Cipollina, A., Di Sparti, M., Tamburini, A., & Micale, G. (2012). Development of a membrane distillation module for solar energy seawater desalination. *Chemical engineering research and design, 90*(12), 2101-2121.

Cipollina, A., Micale, G., & Rizzuti, L. (Eds.). (2009). *Seawater desalination: conventional and renewable energy processes*. Springer Science & Business Media.

Dahdah, T. H., & Mitsos, A. (2014). Structural optimization of seawater desalination: II novel MED–MSF–TVC configurations. *Desalination, 344*, 219-227.

De Andres, M., Doria, J., Khayet, M., Pena, L., & Mengual, J. (1998). Coupling of a membrane distillation module to a multieffect distiller for pure water production. *Desalination, 115*(1), 71-81.

Development, O. M. P. o. G. (2017). World Population Growth, 1750-2100. Retrieved from https://ourworldindata.org/wp-content/uploads/2013/05/updated-World-Population-Growth-1750-2100.png

Druetta, P., Aguirre, P., & Mussati, S. (2014). Minimizing the total cost of multi effect evaporation systems for seawater desalination. *Desalination, 344*, 431-445.

El-Dessouky, H., Alatiqi, I., Bingulac, S., & Ettouney, H. (1998). Steady-state analysis of the multiple effect evaporation desalination process. *Chemical engineering & technology, 21*(5), 437.

El-Dessouky, H. T., & Ettouney, H. M. (2002). *Fundamentals of salt water desalination*. Elsevier.

El-Halwagi, M. M. (2011). *Sustainable design through process integration: fundamentals and applications to industrial pollution prevention, resource conservation, and profitability enhancement*. Elsevier.

El-Halwagi, M. M. (2017). *Sustainable design through process integration: fundamentals and applications to industrial pollution prevention, resource conservation, and profitability enhancement*. Butterworth-Heinemann.

El-Zanati, E., & El-Khatib, K. (2007). Integrated membrane–based desalination system. *Desalination, 205*(1-3), 15-25.

El-Halwagi, M. M. (1992). Synthesis of reverse-osmosis networks for waste reduction. *AIChE Journal, 38*(8), 1185-1198.

Elimelech, M., & Phillip, W. A. (2011). The future of seawater desalination: energy, technology, and the environment. *science, 333*(6043), 712-717.

Elsayed, N. A., Barrufet, M. A., & El-Halwagi, M. M. (2013). Integration of thermal membrane distillation networks with processing facilities. *Industrial & Engineering Chemistry Research, 53*(13), 5284-5298.

Elsayed, N. A., Barrufet, M. A., & El-Halwagi, M. M. (2014). Integration of Thermal Membrane Distillation Networks with Processing Facilities. *Industrial & Engineering Chemistry Research, 53*(13), 5284-5298.

Elsayed, N. A., Barrufet, M. A., & El-Halwagi, M. M. (2015). An integrated approach for incorporating thermal membrane distillation in treating water in heavy oil recovery using SAGD. *Journal of Unconventional Oil and Gas Resources, 12*, 6-14.

Elsayed, N. A., Barrufet, M. A., Eljack, F. T., & El-Halwagi, M. M. (2015). Optimal design of thermal membrane distillation systems for the treatment of shale gas flowback water. *International Journal of Membrane Science and Technology, 2*, 1-9.

Fernandez-Gonzalez, C., Dominguez-Ramos, A., Ibañez, R., & Irabien, A. (2015). Sustainability assessment of electrodialysis powered by photovoltaic solar energy for freshwater production. *Renewable and Sustainable Energy Reviews, 47*, 604-615.

Fiorenza, G., Sharma, V., & Braccio, G. (2003). Techno-economic evaluation of a solar powered water desalination plant. *Energy Conversion and Management, 44*(14), 2217-2240.

Francis, L., Ghaffour, N., Alsaadi, A. A., & Amy, G. L. (2013). Material gap membrane distillation: a new design for water vapor flux enhancement. *Journal of membrane science, 448*, 240-247.

Gabriel, K. J., El-Halwagi, M. M., & Linke, P. (2016). Optimization across the water–energy nexus for integrating heat, power, and water for industrial processes, coupled with hybrid thermal-membrane desalination. *Industrial & Engineering Chemistry Research, 55*(12), 3442-3466.

Gabriel, K. J., Linke, P., & El-Halwagi, M. M. (2015). Optimization of multi-effect distillation process using a linear enthalpy model. *Desalination, 365*, 261-276.

Gabriel, K. J., Noureldin, M., El-Halwagi, M. M., Linke, P., Jiménez-Gutiérrez, A., & Martínez, D. Y. (2014). Gas-to-liquid (GTL) technology: Targets for process design and water-energy nexus. *Current Opinion in Chemical Engineering, 5*, 49-54.

Garcıa-Payo, M., Izquierdo-Gil, M., & Fernández-Pineda, C. (2000). Air gap membrane distillation of aqueous alcohol solutions. *Journal of membrane science, 169*(1), 61-80.

Garcia, D. J., & You, F. (2016). The water-energy-food nexus and process systems engineering: a new focus. *Computers & Chemical Engineering, 91*, 49-67.

Gáspár, F., BALAN, M. C., Jäntschi, L., & ROS, V. (2012). Evaluation of global solar radiation received by a spherical solar collector. *Bulletin UASVM Agriculture, 69*(2), 128-135.

Ghaffour, N., Missimer, T. M., & Amy, G. L. (2013). Technical review and evaluation of the economics of water desalination: current and future challenges for better water supply sustainability. *Desalination, 309*, 197-207.

Glenn, J. C., Gordon, T. J., & Florescu, E. (1997). *State of the Future*. American Council for the United Nations University.

González-Bravo, R., Elsayed, N. A., Ponce-Ortega, J. M., Nápoles-Rivera, F., & El-Halwagi, M. M. (2015). Optimal design of thermal membrane distillation systems with heat integration with process plants. *Applied Thermal Engineering, 75*, 154-166.

Gryta, M., Karakulski, K., & Morawski, A. (2001). Purification of oily wastewater by hybrid UF/MD. *Water research, 35*(15), 3665-3669.

Guijt, C., Meindersma, G., Reith, T., & De Haan, A. (2005). Air gap membrane distillation: 1. Modelling and mass transport properties for hollow fibre membranes. *Separation and purification technology, 43*(3), 233-244.

Hanemaaijer, J. H. (2004). Memstill® — low cost membrane distillation technology for seawater desalination. *Desalination, 168*, 355.

Hou, S. (2008). Two-stage solar multi-effect humidification dehumidification desalination process plotted from pinch analysis. *Desalination, 222*(1-3), 572-578.

Hreinsson, E. B. (2000). *Economies of scale and optimal selection of hydroelectric projects.* Paper presented at Proc. of the IEEE/IEE DRPT2000 Conference, London, U.K. April 4th-7th, 2000.

Ishimaru, N. (1994). Solar photovoltaic desalination of brackish water in remote areas by electrodialysis. *Desalination, 98*(1-3), 485-493.

Iyer, R., & Grossmann, I. E. (1998). Synthesis and operational planning of utility systems for multiperiod operation. *Computers & Chemical Engineering, 22*(7), 979-993.

Kermani, M., Kantor, I. D., & Maréchal, F. (2018). Synthesis of Heat-Integrated Water Allocation Networks: A Meta-Analysis of Solution Strategies and Network Features. *Energies, 11*(5), 1158.

Khawaji, A. D., Kutubkhanah, I. K., & Wie, J.-M. (2008). Advances in seawater desalination technologies. *Desalination, 221*(1-3), 47-69.

Khayet, M. (2011). Membranes and theoretical modeling of membrane distillation: a review. *Advances in colloid and interface science, 164*(1), 56-88.

Khor, C. S., Foo, D. C. Y., El-Halwagi, M. M., Tan, R. R., & Shah, N. (2011). A superstructure optimization approach for membrane separation-based water regeneration network synthesis with detailed nonlinear mechanistic reverse osmosis model. *Industrial and Engineering Chemistry Research, 50*(23), 13444-13456.

Lange, G. (2011). Vacuum-driven MD breakthrough promised by MEMSYS. *International Desalination and Water Reuse Quarterly, 20*(4), 23.

Lokare, O. R., Tavakkoli, S., Khanna, V., & Vidic, R. D. (2018). Importance of feed recirculation for the overall energy consumption in membrane distillation systems. *Desalination, 428*, 250-254.

Mabrouk, A., Elhenawy, Y., Mostafa, G., Shatat, M., & El-Ghandour, M. (2016). Experimental Evaluation of Novel Hybrid Multi Effect Distillation–Membrane Distillation (MED-MD) driven by Solar Energy. *Desalination for the Environment: Clean Water and Energy*, 22-26.

Malcolm, S. A., & Zenios, S. A. (1994). Robust optimization for power systems capacity expansion under uncertainty. *Journal of the operational research society, 45*(9), 1040-1049.

Manne, A. S. (1967). Investment for capacity expansion. *The MIT Press, Cambridge.*

Mapunda, D. W., Chen, S. S., & Yu, C. (2018). The role of informal small-scale water supply system in resolving drinking water shortages in peri-urban Dar Es Salaam, Tanzania. *Applied Geography, 92*, 112-122.

Maravelias, C., Sung, C., & Maravelias, C. T. (2009). A projection-based method for production planning of multiproduct facilities. *AIChE journal*, *55*(10), 2614-2630.

Milow, B., & Zarza, E. (1997). Advanced MED solar desalination plants. Configurations, costs, future—seven years of experience at the Plataforma Solar de Almeria (Spain). *Desalination*, *108*(1-3), 51-58.

Mistry, K. H., Antar, M. A., & Lienhard V, J. H. (2013). An improved model for multiple effect distillation. *Desalination and Water Treatment*, *51*(4-6), 807-821.

Mitra, S., Pinto, J. M., & Grossmann, I. E. (2014). Optimal multi-scale capacity planning for power-intensive continuous processes under time-sensitive electricity prices and demand uncertainty. Part I: Modeling. *Computers & Chemical Engineering*, *65*, 89-101.

Mohamed, E. S., Papadakis, G., Mathioulakis, E., & Belessiotis, V. (2008). A direct coupled photovoltaic seawater reverse osmosis desalination system toward battery based systems—a technical and economical experimental comparative study. *Desalination*, *221*(1-3), 17-22.

Nations, Food and Agriculture Organization of the United Nations (2014). Water Withdrawal Retrieved from http://www.fao.org/nr/water/aquastat/infographics/Withdrawal_eng.pdf

Neebe, A., & Rao, M. (1986). Sequencing capacity expansion projects in continuous time. *Management Science*, *32*(11), 1467-1479.

Ng, K. C., Thu, K., Oh, S. J., Ang, L., Shahzad, M. W., & Ismail, A. B. (2015). Recent developments in thermally-driven seawater desalination: Energy efficiency improvement by hybridization of the MED and AD cycles. *Desalination*, *356*(Supplement C), 255-270.

Ophir, A., & Lokiec, F. (2004). *Review of MED fundamentals and costing.* Paper presented at the Proc. of the International Conference on Desalination Costing. December, 2004.

Ortiz, J., Expósito, E., Gallud, F., García-García, V., Montiel, V., & Aldaz, A. (2008). Desalination of underground brackish waters using an electrodialysis system powered directly by photovoltaic energy. *Solar Energy Materials and Solar Cells*, *92*(12), 1677-1688.

Population Growth Rate: Saudi Arabia. (2017). Retrieved from https://www.google.com/publicdata/explore?ds=d5bncppjof8f9_&met_y=sp_pop_grow&idim=country:SAU:PAK:SYR&hl=en&dl=en

Qtaishat, M., Matsuura, T., Kruczek, B., & Khayet, M. (2008). Heat and mass transfer analysis in direct contact membrane distillation. *Desalination*, *219*(1-3), 272-292.

Rachford, T. M., Scarato, R. F., & Tchobanoglous, G. (1969). Time-capacity expansion of waste treatment systems. *Journal of the Sanitary Engineering Division*, *95*(6), 1063-1078.

Rijsberman, F. R. (2006). Water scarcity: Fact or fiction? *Agricultural Water Management*, *80*(1), 5-22.

Sadhishkumar, S., & Balusamy, T. (2014). Performance improvement in solar water heating systems—A review. *Renewable and Sustainable Energy Reviews, 37*, 191-198.

Saffarini, R. B., Summers, E. K., & Arafat, H. A. (2012). Economic evaluation of stand-alone solar powered membrane distillation systems. *Desalination, 299*, 55-62.

Sahinidis, N. V., Grossmann, I. E., Fornari, R. E., & Chathrathi, M. (1989). Optimization model for long range planning in the chemical industry. *Computers & Chemical Engineering, 13*(9), 1049-1063.

Sajjad, M., & Rasul, M. G. (2015). Simulation and optimization of solar desalination plant using Aspen Plus simulation software. *Procedia Engineering, 105*, 739-750.

Samanta, B., & Al Balushi, K. R. (1998). Estimation of incident radiation on a novel spherical solar collector. *Renewable Energy, 14*(1-4), 241-247.

Scarato, R. F. (1969). Time-capacity expansion of urban water systems. *Water Resources Research, 5*(5), 929-936.

Schrage, L. E. (2006). *Optimization modeling with LINGO*: Lindo System.

Shahzad, M. W., Ng, K. C., Thu, K., Saha, B. B., & Chun, W. G. (2014). Multi effect desalination and adsorption desalination (MEDAD): A hybrid desalination method. *Applied Thermal Engineering, 72*(2), 289-297.

Sharaf, M., Nafey, A., & García-Rodríguez, L. (2011). Thermo-economic analysis of solar thermal power cycles assisted MED-VC (multi effect distillation-vapor compression) desalination processes. *Energy, 36*(5), 2753-2764.

Shuhaibar, Y. K. (1972). Staging of investment in desalination facilities and associated storage facilities (Doctoral dissertation, The University of Arizona).

Skiborowski, M., Mhamdi, A., Kraemer, K., & Marquardt, W. (2012). Model-based structural optimization of seawater desalination plants. *Desalination, 292*, 30-44.

Souhaimi, M. K., & Matsuura, T. (2011). *Membrane distillation: principles and applications*. Elsevier.

Subramani, A., Badruzzaman, M., Oppenheimer, J., & Jacangelo, J. G. (2011). Energy minimization strategies and renewable energy utilization for desalination: a review. *Water research, 45*(5), 1907-1920.

Vince, F., Marechal, F., Aoustin, E., & Bréant, P. (2008). Multi-objective optimization of RO desalination plants. *Desalination, 222*(1-3), 96-118.

Wang, P., & Chung, T.-S. (2012). A conceptual demonstration of freeze desalination–membrane distillation (FD–MD) hybrid desalination process utilizing liquefied natural gas (LNG) cold energy. *Water research, 46*(13), 4037-4052.

Water-Technology. Ras Al Khair Desalination Plant, Saudi Arabia. Retrieved from http://www.water-technology.net/projects/-ras-al-khair-desalination-plant/

Zamen, M., Amidpour, M., & Soufari, S. (2009). Cost optimization of a solar humidification–dehumidification desalination unit using mathematical programming. *Desalination, 239*(1-3), 92-99.

Zuo, J., Bonyadi, S., & Chung, T.-S. (2016). Exploring the potential of commercial polyethylene membranes for desalination by membrane distillation. *Journal of membrane science, 497*, 239-247.